RMetS
Royal Meteorological Society

A multi-scale analysis of the extreme rain event of Ouagadougou in 2009

Jean-Philippe Lafore,[a*] Florent Beucher,[a] Philippe Peyrillé,[a] Aïda Diongue-Niang,[b] Nicolas Chapelon,[c] Dominique Bouniol,[a] Guy Caniaux,[d] Florence Favot,[a] Frédéric Ferry,[e] Françoise Guichard,[a] Emmanuel Poan,[a] Romain Roehrig[d] and Théo Vischel[f]

[a]*CNRM-UMR3589/GMME, Météo-France and CNRS, Toulouse, France*
[b]*ANACIM/MET, Dakar, Senegal*
[c]*DP/CISMF, Météo-France, Toulouse, France*
[d]*CNRM-UMR3589/GMGEC, Météo-France and CNRS, Toulouse, France*
[e]*ENM/ER, Météo-France, Toulouse, France*
[f]*Université Grenoble Alpes, IRD, CNRS, G-INP, IGE, 38000 Grenoble,France*

*Correspondence to: J.-P. Lafore, CNRM Météo-France, 42 Av. G. Coriolis, 31057 Toulouse Cedex 7, France. E-mail: jean-philippe.lafore@meteo.fr

This study presents a multi-scale analysis of an extreme rain event that occurred in Burkina Faso on 1 September 2009 with an absolute record of 263 mm rainfall observed at Ouagadougou. This high-impact weather system results from the combination of several favourable ingredients at different scales. The sea-surface temperature anomaly patterns in July–August 2009 of both the Atlantic cold tongue, the Tropical Atlantic Dipole and the Mediterranean Sea are favourable factors for the northward penetration of the West African monsoon. The intense convective activity of the last 10-day period in August is associated with the crossing of a convectively coupled Kelvin wave increasing the African easterly wave (AEW) activity, and of an equatorial Rossby wave.

At the synoptic scale this event corresponds to the passage of a train of three AEWs with increasing magnitude. Behind the first AEW trough axis, an intense and deep southerly monsoon burst develops. It contributes to the amplification of the second AEW and its breaking is associated with the formation of an intense meso-vortex on the southern flank of the African easterly jet. Compared to the fast-moving squall line, the dominant type of precipitating weather system over the Sahel, the Ouagadougou precipitating system appears to be a moist vortex propagating slowly, allowing rainfall accumulation, without wind gusts or convective cold pools observed at the surface. The main precipitation area is located about 2° longitude downshear (westward due to the African easterly jet) of the centre of this strong meso-vortex.

Key Words: high-impact weather system; West Africa; African easterly waves; convection

Received 24 February 2017; Revised 8 September 2017; Accepted 15 September 2017; Published online in Wiley Online Library 29 November 2017

1. Introduction

The African continent is repeatedly affected by high-impact weather (HIW) with devastating consequences for local communities. Life and property losses, damage to infrastructure (roads, bridges and buildings) and resources (energy, water supply and health sector) have been reported over the years because of HIW. In the 1970s and 1980s severe droughts prevailed over the Sahel (Nicholson, 2001) causing famine and considerable economic losses (Benson and Clay, 1998). Within the current period of partial rainfall recovery (Lebel and Ali, 2009; Panthou *et al.*, 2014), West African countries have been struck in the past decade by several floods of unprecedented magnitude (Descroix *et al.*, 2012; Nka *et al.*, 2015). It is the severe 2007 flood in sub-Saharan countries that brought HIW flood events to the attention of the world (Levinson and Lawrimore, 2008). According to the gauge-only gridded precipitation dataset (PREC/L) of the Climate Prediction Center, a part of the National Oceanic and Atmospheric Administration (NOAA), the 2012 rainfall season was the wettest since 1952 (Thiaw, 2013). The torrential rains and associated persistent flooding hit the western Sahel hardest in areas that included western Mali, the southern half of Senegal, and the Guineas. Many extreme events were reported. For instance the station of Dakar registered record-breaking precipitation of

© 2017 Royal Meteorological Society

152 mm on 26 August (Diongue-Niang *et al.*, 2017; personal communication). Also in 2012, the middle Niger River exhibited the highest flood level ever registered from the beginning of its monitoring in 1929 (Sighomnou *et al.*, 2013).

A key question is to understand what determines the predictability of these events, for which both individual cases and statistical studies are needed. In the framework of THORPEX* (THe Observing Research and Predictability Experiment), the THORPEX-Africa regional committee has selected a few cases related to flooding events to study their predictability. To achieve this task, three steps have been defined: (i) description and conceptual model of case-studies, (ii) verification of forecasts and the assessment of model ability to predict such events, (iii) modelling studies to further analyse the predictability of such events. This article aims at tackling the first item for the case-study selected for the West African subregion. It is part of a wet spell in the Sahel with an extreme rainfall event that occurred in Ouagadougou (Burkina Faso) on 1 September 2009, with 263 mm recorded in ten hours. This led to 150 000 people being displaced (of 1.5 million inhabitants), 9 deaths, extensive loss of property and damaged roads.

Several observational and numerical studies have been performed to document and better understand rainfall events in West Africa. They are based on case-studies from field campaigns such as Convection Profonde Tropicale 1981 (COPT81: Chong *et al.*, 1987; Redelsperger and Lafore, 1988; Roux, 1988), Hydrological Atmospheric Pilot Experiment (HAPEX-Sahel: Diongue *et al.*, 2002; Redelsperger *et al.*, 2002), or more recently the African Monsoon Multidisciplinary Analysis (AMMA) SOP2006. Case-studies such as presented in Barthe *et al.* (2010), Chong (2010), Schwendike and Jones (2010), Birch *et al.* (2013) and Beucher *et al.* (2014) focused more particularly on the interactions between mesoscale systems and synoptic disturbances such as African easterly waves (AEWs) which are key synoptic weather systems affecting West Africa during the monsoon (Fink and Reiner, 2003). These studies mainly addressed fast-moving squall lines that are the dominant type of rain event over the semi-arid Sahel region (Mathon *et al.*, 2002). They contribute up to 80% of the annual regional rainfall over the Sahel (D'Amato and Lebel, 1998; Le Barbé *et al.*, 2002). They often generate intense precipitation and strong wind bursts associated with intense cold pools fed by rain evaporation. Nevertheless due to their fast propagation, the passage of a squall line over a given location is short, typically from about 1/2 to 2 h for the convective and stratiform parts, respectively (see the recent mesoscale convective systems (MCS) statistics over West Africa of Lafore *et al.* (2017, Fig. 3.16)). This short duration may explain why the observed accumulated rainfall rarely exceeds the precipitable water (PW) ahead of the squall line, typically 50–65 mm over the Sahel during the monsoon season (Poan *et al.*, 2013). For instance the maximum accumulated precipitation totals recorded were 47 and 37 mm for the passage of a squall line during the COPT81 and HAPEX-Sahel field experiments, respectively (Chalon *et al.*, 1988; Redelsperger *et al.*, 2002), whereas the PW ahead of the squall line was about 55 mm for both cases. Le Barbé *et al.* (2002) found a mean accumulated rainfall per MCS of ∼15 mm at Niamey. To reach a daily accumulated rainfall above PW, the system must be very efficient in concentrating water vapour for a long duration at a given location due either to a slow propagation, a forcing mechanism by the topography or the large-scale dynamics. As observed extreme rainfall events reach values above 100 mm per day at a given location (Panthou *et al.*, 2012), it raises the following questions: Are the physical processes involved in Sahelian extreme rain events different from the ones involved in squall lines? What are their temporal and spatial scales?

There is, however, a lack of studies of such HIW rain events to help answer these questions. Among the few related studies, Paeth *et al.* (2011) performed an analysis of the 2007 flood caused by a sequence of strong rain events in August and September. They first assessed the structure and intensity of the flood and of associated rain event sequences from various observational datasets. Estimated return times from the Tropical Rainfall Measuring Mission (TRMM) range between 1 and 50 years for daily precipitation, but have a high spatial heterogeneity and a maximum over the Upper Volta Basin. Burkina Faso appears as a hot spot for flood-producing rain events from August to September.

Another question is: What are the contextual elements of the climate conditions in which HIW rain events may occur? To help answer this question, Nicholson (2009) proposed a conceptual framework for studying rainfall variability over West Africa resulting from two distinct modes: *latitudinal displacements* of the tropical rain belt and changes in its *intensity*. From this arise four patterns of rainfall anomalies: 'non-dipole' years when anomalies are of the same sign over most of West Africa due to a change in rain-belt intensity, whereas anomalies are of opposite sign in the Sahel and the Guinea Coast during 'dipole' years due to latitudinal displacements (see Fig. 1 of Nicholson (2009)). In this framework, 2007 is a 'wet non-dipole' year (Paeth *et al.*, 2011), whereas 2009, 2012 and 2013 are 'wet dipole' years (see State of Climate in corresponding years: Thiaw, 2013).

The above framework proposes some large-scale factors favouring wet or dry years for the West African monsoon (WAM), but we do not know if the probability of occurrence of HIW rain events is stronger during wet years than in dry years. Also, these HIWs are not excluded from a dry year. So far there is no clear understanding of the atmospheric conditions leading to an HIW rain event.

At the regional scale, Crétat *et al.* (2015) analysed the relationship between AEW and daily rainfall over West Africa and concluded that 3–5-day AEWs establish the most favourable synoptic conditions for the development of intense rainfall events. This is consistent with previous work showing that the AEW activity is enhanced during wet years (Grist, 2002; Grist *et al.*, 2002; Nicholson, 2009; Paeth *et al.*, 2011). Ventrice and Thorncroft (2013) showed that the AEW activity increases at the leading edge and during the convectively active phase of strong convective coupled Kelvin waves (CCKWs). Ventrice *et al.* (2011) also suggested that the Madden–Julian Oscillation (MJO: Madden and Julian, 1971) directly influences AEW activity. During MJO phases 8, 1 and 2, diagnosed by the Wheeler and Hendon (2004) Real-time MJO Multivariate (RMM) index, the African easterly jet (AEJ) increases and convection is enhanced over tropical Africa, whereas AEW activity is locally enhanced during phases 1–3. According to these studies, equatorial waves (CCKW and MJO at least) can modulate the environment on which AEWs develop, i.e. the magnitude of the AEJ, the vertical wind shear, the low-level convergence and vorticity patterns. Since the AEWs are the leading driver of the most intense storms, a connection is possible between equatorial waves and HIW. The present article actually shows that this link exists, which opens up interesting forecasting perspectives (see section 4).

If a better understanding of extreme rainfall events is a crucial issue in better forecasting them, another issue is the trend in their occurrence and intensity in the context of ongoing global warming (Westra *et al.*, 2014). At a regional scale, in the Sahel, Panthou *et al.* (2014) found that the partial recovery of rainfall is more likely due to the increase in the number of intense events (increase of 33% between 1970–1990 and 2001–2010), than the increase in the total number of events (3% of increase in the same periods). Taylor *et al.* (2017) also found that the frequency of extreme Sahelian storms tripled since 1982 in satellite observations.

The main goal of this first article is to present a multi-scale analysis of the extreme rain event of Ouagadougou that occurred on 1 September 2009, with a focus on regional and synoptic scales and to identify key factors for this type of event. This case has been used in the recently published West African Forecaster's Handbook (Parker and Diop-Kane, 2017) to

*www.wmo.int/thorpex.

illustrate AEW breaking events (Cornforth *et al.*, 2017) as seen by forecasters. In a companion article we will analyse the physical mechanisms involved in the small-scale development of a moist vortex associated with this extreme rain event, owing to the computation of budgets of heat, moisture and vorticity from a convection-permitting simulation.

After a description in section 2 of the datasets used in this study, section 3 describes the characteristics of this extreme event and the large-scale context it is embedded in. Section 4 focuses on wave activity, more specifically on AEWs and on the impact of equatorial waves on this event. The convective organization is analysed in section 5. Section 6 summarizes the main findings and proposes a list of factors favouring the occurrence of this type of event associated with the breaking of an AEW.

2. Data and analysis methods

2.1. Observations

In the framework of THORPEX-Africa, daily rain-gauge data of a network of 579 stations have been kindly provided by National Weather Services of most West African countries impacted by this wet spell. These rain-gauge network data cover a 20-day period centred on 1 September 2009 to document this period of intense precipitation (see subsection 3.1) in which the Ouagadougou event is embedded.

This dataset is very valuable for the present study and for further ones to assess the numerical weather prediction (NWP) system's skill in forecasting such extreme events. In addition, TRMM-3B42 rainfall estimates (Huffman *et al.*, 2007) have been used. To complement this, the Global Satellite Mapping of Precipitation (GSMaP) v5 satellite estimate of $0.1^\circ \times 0.1^\circ$ gridded 1 h accumulated precipitation (Ushio *et al.,* 2009) is used to track MCSs.

The convective activity and its spatial structure have been analysed by computing the polarized corrected temperature (PCT) parameter (Mohr and Zipser, 1996) from snapshots provided by AMSR-E (Advanced Microwave Scanning Radiometer - Earth observing system), SSM/I (Special Sensor Microwave Imager) and TMI (TRRM Microwave Imager) microwave radiometers. PCT also allows the identification of convective and stratiform regions. Daily-averaged outgoing long-wave radiation (OLR) data provided by the National Oceanic and Atmospheric Administration (NOAA) polar-orbiting satellites (Liebmann and Smith, 1996) was used as a proxy for convective activity.

To assess the oceanic state in 2009, sea-surface temperature (SST) anomalies during July–August 2009 have been computed from the Reynolds climatology over the 33-year period 1982–2014 (Reynolds *et al.*, 2002). The soundings of Abidjan (5.18°N, 4°W) performed twice a day have been used to assess the presence of equatorial waves.

2.2. Reanalysis

The present study is partly based on the last ('Interim') European Centre for Medium-Range Weather Forecasts (ECMWF) Reanalysis (Dee *et al.*, 2011, ERA-I hereafter). To improve the analysis in a region of sparse observations such as Africa, we assimilated remote-sensing microwave data from Advanced Microwave Sounding Unit AMSU-B, by using the method developed by Karbou *et al.* (2010a) as in Beucher *et al.* (2014). We performed a 4D-Var assimilation with the global Action des Recherches Petite Echelle et Grand Echelle (ARPEGE) operational model of Météo-France (Courtier *et al.,* 1994). The 4D-Var assimilation experiment was performed over a ~1-month period (13 August to 10 September 2009), four times per day, with the April 2010 version (T798 truncation and a stretched horizontal grid allowing ~15 km resolution over Africa). Thanks to its finer horizontal resolution and AMSU-B data, we used the ARPEGE reanalysis in this article for a more accurate analysis of the synoptic scale in section 4 (see Karbou *et al.* (2010b) and Beucher *et al.* (2014) for a comparison between ERA-I and ARPEGE), in addition to ERA-I.

2.3. Analysis methods

As done for instance by Takayabu (1994) or Wheeler and Kiladis (1999), a zonal space–time spectral analysis is performed to detect and analyse equatorial waves concomitant with the present extreme precipitation event. Following Roundy and Franck (2004) and Schreck *et al.* (2012), the spectral analysis is made for each latitude between 30°S and 30°N and filtered in the wave-number–frequency domain without imposing equatorial symmetry to the data. Table 1 summarizes the characteristics of the filters used to extract the Madden–Julian Oscillation (MJO), Kelvin (K), equatorial Rossby (ER), and westward mixed Rossby–gravity (MRG) waves. We added the tropical-depression-type (TD-type) disturbances that correspond to AEWs over Africa. The filtering is applied to either the 200 hPa velocity potential seasonal anomalies, OLR seasonal anomalies or the mass-weighted 950–600 hPa layer-averaged meridional wind (hereafter meridional mass transport) depending on the wave type (Table 1). The equivalent depths used for the wave filtering are 8–90 m for ER, Kelvin and MRG (Wheeler and Kiladis, 1999) while no equivalent depth is imposed for the MJO and TD-AEW.

We developed an AEW tracking based on the barotropic flow (mass-weighted mean wind between 950 and 600 hPa) as a two-step procedure: (i) the detection of the maximum relative vorticity providing a 'first guess' for the tracked pattern, (ii) a finer spatial localisation by searching for the minimum wind speed corresponding to the centre of the barotropic flow. This method is applied at an hourly frequency to ARPEGE reanalysis and simulations, at 15 km horizontal resolution (see section 5).

3. Main characteristics of the extreme event and large-scale context

3.1. Precipitation

The case-study occurred during a wet spell that affected the whole Sahel during the 20-day period from 21 August to 10 September 2009, marked with heavy precipitation leading to floods in many Sahelian countries (notably in Niger, Senegal, Mauritania, Gambia – see State of Climate in 2009, Arndt *et al.* (2010)). The event that occurred in Burkina Faso on 1 September, caused by a slow-moving MCS (see section 5), has been the most extreme ever observed over the western Sahel. Between 0400 and 1600 UTC 263 mm were recorded at Ouagadougou, the capital city. The accumulated hourly rainfall peak (97 mm) occurred between 0700 and 0800 UTC. The 30 rain records collected over Burkina Faso on 31 August and 1 September (Figure 1(a)) provide an idea of the size, intensity and trajectory of this extreme event. The pattern of the corresponding accumulated rain as estimated by TRMM (red isolines) is in agreement with rain-gauge records, although underestimated (by a factor 2 for the maximum) probably partly due to the difference in scale. The Ouagadougou extreme event affected an area of about $150 \times 100\,\mathrm{km}^2$ with accumulated rain above 75 mm (50 mm for TRMM). For the 15 stations at a distance less than 1° from Ouagadougou, the mean accumulated rainfall was 94 mm (117 mm for the seven stations at a distance less than 0.5°) and the second highest record reached 213 mm at Boulbi (13 km south of Ouagadougou). TRMM estimates reached a maximum of 110 mm close to Ouagadougou. TRMM suggests that this event also generated important precipitation (above 75 mm) during the previous night over eastern Burkina, but the density of the rain-gauge network was too sparse to confirm this finding. Figure 1(b) shows observed extrema of daily precipitation over West Africa during the 20-day period from 21 August to 10 September, with the indication of values above 100 mm day^{-1} (red points) and

Table 1. Characteristics of the filters in the space–time spectral domain used to extract main types of equatorial waves.

Wave type	Propagation	Period T (days)	Zonal wave number k	Zonal wavelength range (km)	Variables from ERA-I
MJO	Eastward	30–96	1-5	8000–40 000	VP_{200}, OLR, V_m
Kelvin	Eastward	25–30	1-14	2800–40 000	VP_{200}, OLR, V_m
ER	Westward	9.7–48	1-10	4000–40 000	VP_{200}, OLR, V_m
MRG	Westward	3–96	1-10	4000–40 000	V_m
TD-type (AEW)	Westward	2–5	6-20	2000–6600	V_m

These filters are similar to those of Roundy and Frank (2004) (see their Fig. 4 for illustration). Depending on the wave type, the filtering is applied to different ERA-I variables: velocity potential at 200 hPa (VP_{200}), OLR and the meridional mass transport (V_m) defined as the mass-weighted 950–600 hPa layer-averaged meridional wind.

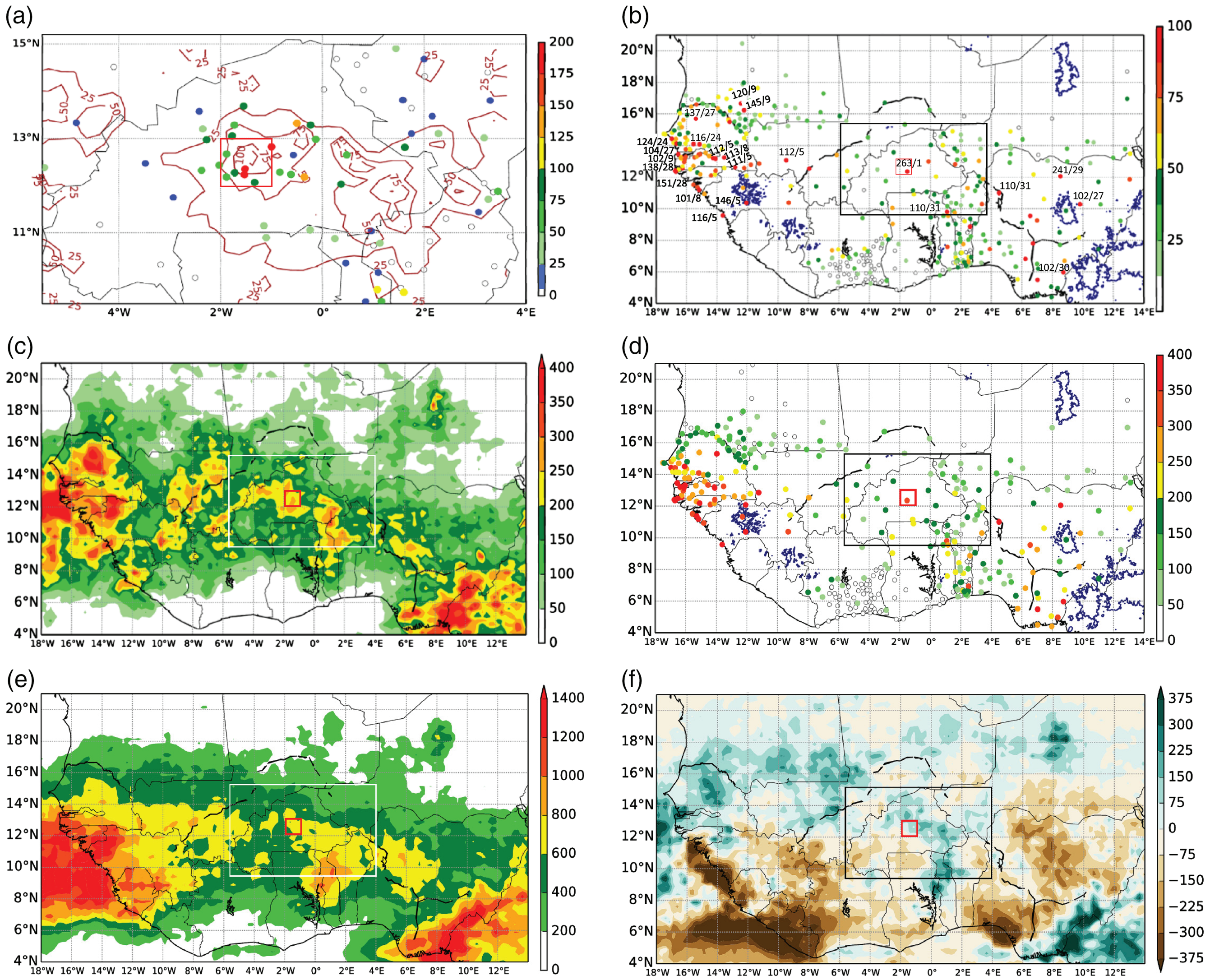

Figure 1. (a) Two-day accumulated precipitation (mm) over Burkina Faso from 31 August at 0600 UTC to 2 September 2009 at 0600 UTC as observed (coloured points) and as estimated by TRMM (red isolines). (b) Observed extrema of daily precipitation over West Africa during the 20-day period from 21 August to 10 September. Values above 100 mm day^{-1} (red points) are indicated with the date of occurrence, for instance 120/9 means 120 mm observed on 9 September. (c) and (d) Accumulated precipitation (mm) over the same 20-day period as estimated by TRMM and observed, respectively. (e) Accumulated TRMM precipitation (mm) in JAS 2009 and (f) its anomaly (mm) from the 1998 to 2014 TRMM climatology. The 1° square around Ouagadougou is outlined in red in all panels, and the Burkina Faso zoom of panel (a) is superposed on all other panels in black or white.

their date of occurrence. The Ouagadougou case is the absolute observed maximum (263 mm with a return period estimated at 10 000 years by Karambiri (2009)) of the 22 recorded strong events. Here, we consider that an event is strong when the daily precipitation reaches more than 100 mm, i.e. when it produces much more precipitation than the amount of water vapour stored in the column (PW_{max} ~65 mm: Poan *et al.*, 2013; Lafore *et al.*, 2017). This is likely a large number as Panthou *et al.* (2012) estimate that the return time for a 100 mm daily precipitation is 15 and 20 years at Ouagadougou and Niamey, respectively. Those strong events in 2009 are clustered over specific regions (Senegal, the south of Mauritania in particular) and periods corresponding to the passage of AEWs as shown later, in section 4.1. The TRMM accumulated rain over this 20-day period (Figure 1(c)) agrees well with rain-gauge observations (Figure 1(d)) at this scale. It is to be noticed that regions with intense daily events (Figure 1(b)) correspond to regions of maximum accumulated rain over the 20-day period, suggesting a major contribution of intense events to the seasonal rainfall (which is consistent with Panthou *et al.* (2012)). Figure 1(e) shows the TRMM accumulated rainfall at the monsoon seasonal scale (July–August–September, JAS hereafter) and Figure 1(f) its anomaly relative to the 1998–2014 TRMM climatology. Clearly 2009 appears as a wet dipole year over the Sahel (up to ∼+300 mm). At the seasonal scale the rainfall anomalies are located over Senegal, the south of Mauritania, Mali and Niger, where intense events (above 100 mm day^{-1})

© 2017 Royal Meteorological Society

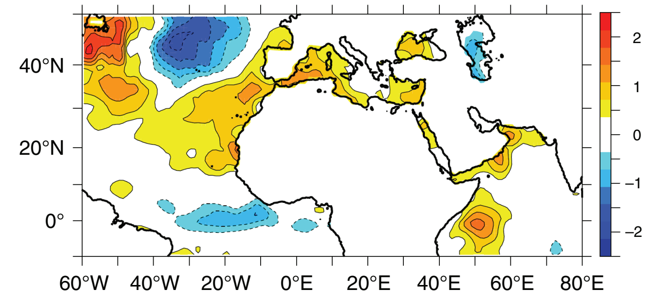

Figure 2. SST anomalies (°K) during July–August 2009 from the Reynolds climatology over the 32-year period 1982–2014.

occurred during the active 20-day period of August and September (Figure 1(d)), suggesting a significant contribution of intense events to the seasonal rainfall anomaly.

3.2. *SST pattern*

At very large scale, 2009 was characterized by the transition between a waning Pacific La Niña and the establishment of a strong El Niño event from June 2009 to April 2010 (Arndt *et al.*, 2010). In 2009, the Atlantic Ocean was warmer in the Northern Hemisphere due to the warm phase of the Atlantic Multi-decadal Oscillation (AMO: Enfield and Mestas-Nunez, 1999) which has resulted in greater Atlantic hurricane activity since 1995.

Figure 2 displays SST anomalies surrounding Africa for July–August 2009. A dipole is present in the North Atlantic with warm anomalies (2 °C) in the northwestern Atlantic and anomalies colder than −2 °C eastward. The cold anomalies in the northeastern Atlantic are the signature of a negative North Atlantic Oscillation (NAO) index for the July–August period. In the tropical Atlantic, a positive Atlantic dipole (Lamb, 1978; Parker *et al.*, 1988; Servain, 1991) is present with a cold anomaly (down to −1 °C) along the Equator, which also affects the Atlantic cold tongue in the eastern equatorial basin. Based on the climatological indices defined by Caniaux *et al.* (2011), the cold tongue was colder and more extended in July–August 2009 than the climatology (not shown). Combined with the AMO warm phase, a colder Atlantic cold tongue and a resulting positive tropical Atlantic SST dipole are favourable conditions for the northward penetration of the WAM into the West African continent. The warm anomaly in the Mediterranean Sea (Figure 2) can also be considered as a favourable factor (Rowell, 2003; Peyrillé *et al.*, 2007).

The warm SST anomaly in the Indian Ocean (Figure 2) started at the same time as the Pacific El Niño in 2009, instead of one year later as more commonly found (e.g. in 1998, 1987 and 1983: Arndt *et al.*, 2010). A statistical relationship has been found linking a warm anomaly in the Indian Ocean to dry conditions over the Sahel in the last decades (Bader and Latif, 2003; Giannini *et al.*, 2003), such that the warm anomaly over the Indian Ocean should not have favoured moister conditions over the Sahel in 2009. Recent studies indicate, however, that this link might not be straightforward for the last decade with the recent phasing of the NAO and El Niño/Southern Oscillation (ENSO) (Joly *et al.*, 2007; Rodriguez-Fonseca *et al.*, 2011).

To summarize, the SST anomaly patterns in July–August 2009 of the Atlantic cold tongue, the Tropical Atlantic Dipole and the Mediterranean Sea are favourable factors for the WAM northward penetration. They are consistent with the classification of 2009 as a 'dipole wet year' (Nicholson, 2009). However, the impacts of El Niño, Indian Ocean warming and negative NAO on the WAM deserve more analysis.

3.3. *Multi-scale nature of the event*

Figure 3(a) analyses the seasonal evolution of the TRMM mean rainfall in 2009 in the 1° square around Ouagadougou (12–13°N;

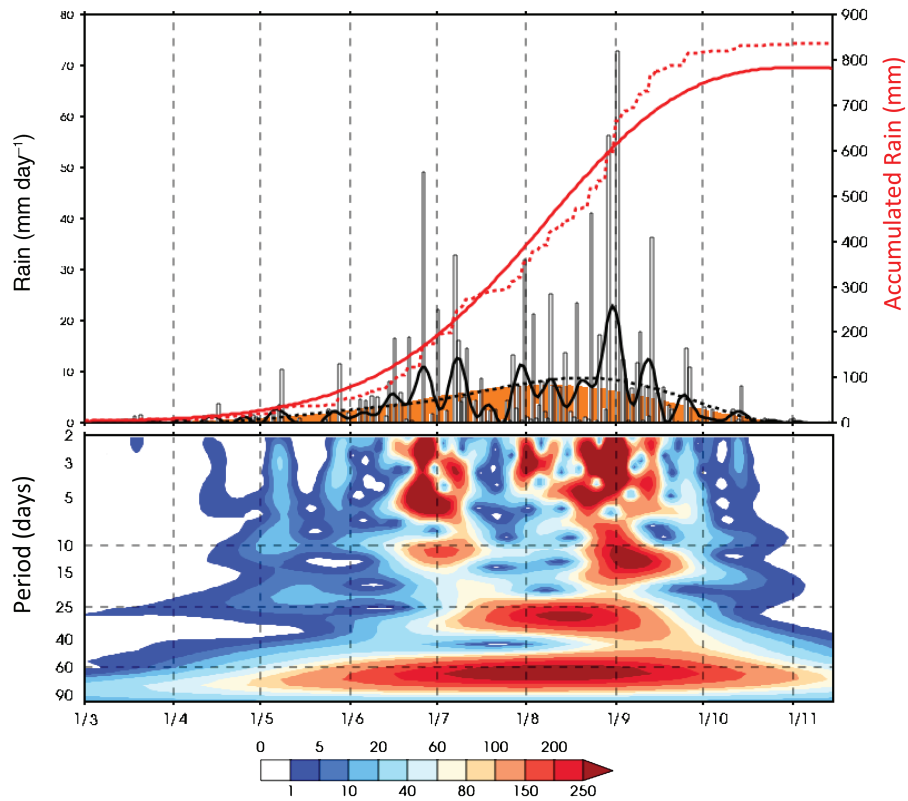

Figure 3. (a) TRMM precipitation evolution for the year 2009 (mm day^{-1}), averaged over a 1° square around Ouagadougou (12–13°N, 1–2°W, red square in Figure 1). Raw daily data are indicated with white bars. The orange shaded area corresponds to the climatological (1998–2013) annual cycle. The 2009 annual cycle is indicated with the dashed black curve and obtained with a 90-day low-pass spectral filter applied on raw precipitation. The intraseasonal scale is emphasized with a solid black curve and obtained with a 10-day low-pass spectral filter. Red curves correspond to the accumulated rain (mm) since 1 January for the climatology (solid red line) and the year 2009 (dashed red line). (b) Wavelet analysis of TRMM precipitation averaged over the 1° square around Ouagadougou and 90-day high-pass filtered.

2–1°W, red square in Figure 1). The passage of the extreme Ouagadougou event is clearly seen at the daily and box scales (up to 72 mm day^{-1}). This extreme rain event significantly contributes to the positive anomaly of accumulated rain observed in 2009 at Ouagadougou. Another active period is observed from late June to early July. When compared to the TRMM (1998–2012) climatology, 2009 rainfall is weaker in June and July, which corresponds to a late onset, but the deficit is made up and reversed during the very active period of August–September. The wavelet analysis (Figure 3(b)) reveals that four bands are active at synoptic (3–5 days), short (10–15 days), medium (20–30 days) and long (40–80 days) intraseasonal scales. The Ouagadougou extreme event thus occurs at a time when all these scales of variability are strong (this is also true of the active period of late June–early July). It suggests that this extreme event corresponds to the superposition of favourable conditions at different temporal scales.

4. Propagating modes of variability and wave activity

4.1. AEWs

Figure 4 provides a synoptic view of the Ougadougou event over a 3-day period at two key levels to identify AEWs: at low levels (925 hPa, right) and at the AEJ level (700 hPa, left). At 700 hPa the AEJ is well defined in the 10–20°N band with a maximum intensity above 20 m s^{-1} (Figures 4(a)–(c)). Its oscillations correspond to a train of three AEWs, and increase during this 3-day period. On 30 August, the first AEW of this series is well formed with its trough T1 located over Burkina Faso (red line in Figure 4(a)). A fast-moving squall line propagates ahead of T1 in the AEJ core (pink shading). The trough T1 propagates westward and reaches the coast two days later. An important feature at 700 hPa is the development of a strong southerly flow behind T1 coming from the Southern Hemisphere. The signature at low levels is a westerly flow west of T1 and an intense southwesterly monsoon flow east of T1 (Figures 4(d)–(f)). The combination of these strong southerlies behind T1 at low levels and at the AEJ level is a deep southerly burst maximum on 31 August. This is associated with the development of a deep and strong ridge R1 (dotted red line in Figure 4) behind T1. Quite unusually, this southerly burst is so strong that it brings dry air from the Southern Hemisphere and generates a dry anomaly (dark shading in Figures 4(d)–(f)) in the R1 region.

A second wave develops behind this first AEW (T1 and R1). Its trough T2 appears just west of Lake Chad on 30 August

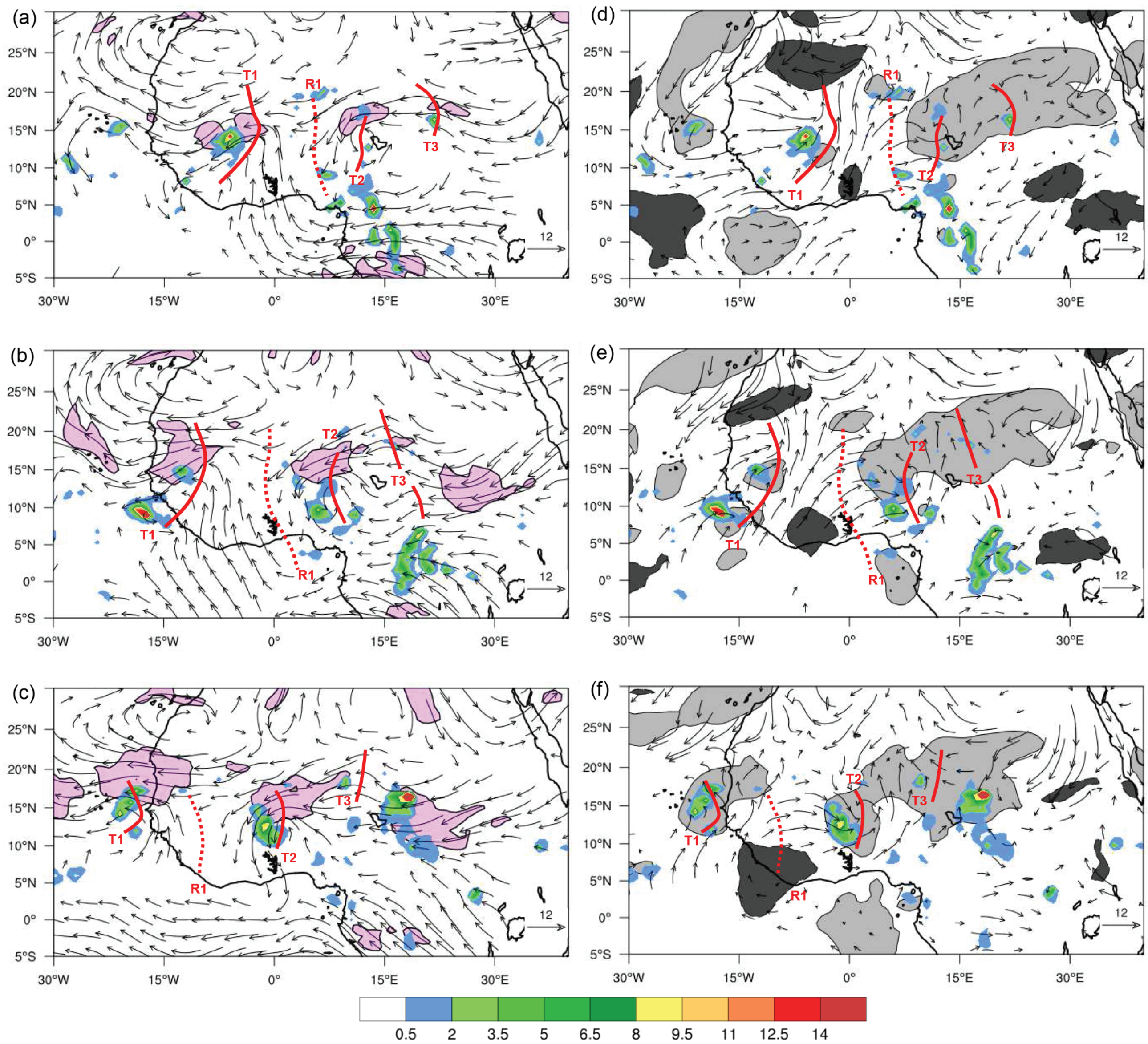

Figure 4. Maps of the horizontal wind vector (a–c) at 700 hPa stronger than 5 m s^{-1}, and (d–f) at 925 hPa stronger than 2.5 m s^{-1}. At 700 hPa light pink shading for wind speed above 12 m s^{-1} (a–c) outlines the AEJ cores, whereas at 925 hPa anomalies of precipitable water PW are superposed to highlight moister patches (>5 mm light grey shading) and drier patches (<5 mm dark grey one). For all panels, precipitation rates (mm h^{-1}) are marked with colour shading. Data from ERA-I are shown at 0600 UTC on (a, d) 30 August, (b, e) 31 August and (c, f) 1 September. The location of troughs T1, T2 and T3 (red solid lines) and ridge R1 (red dashed line) are marked in all panels.

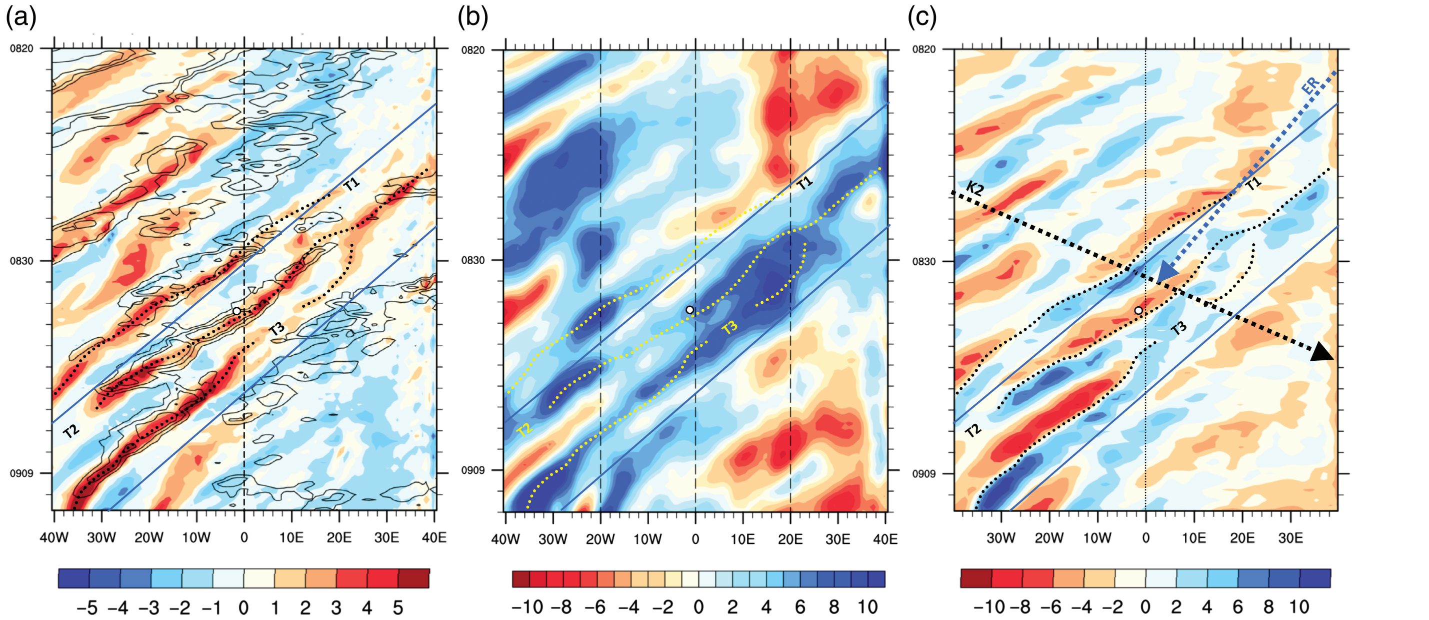

Figure 5. Longitude–time (month+day) diagrams between 40°W and 40°E from 20 August to 10 September 2009 for: (a) vorticity (10^{-5} s^{-1}) at 700 hPa, (b) precipitable water anomaly PW (mm) and (c) meridional mass transport (m s^{-1}) defined as the mass-weighted 950–600 hPa layer-averaged meridional wind. Fields are extracted from the ERA-I reanalysis and averaged in the 10–18°N band. Zonal wind averaged over the 700–600 hPa layer is superimposed on panel (a) only for strong easterlies to highlight the AEJ intensity (isolines between −15 and −20 m s^{-1} with a 2.5 m s^{-1} interval). Also the trough of each AEW (labelled from T1 to T3) corresponding to the line of maximum vorticity is superposed on all panels (dotted black or yellow lines). The passage of the wet spell corresponding to a band of positive PW anomaly (b), is outlined by the blue lines on all panels. The white dot indicates the location of the Ouagadougou event. The black and blue heavy dashed arrows superposed on panel (c) correspond to the track of the Kelvin (K2) and Rossby (ER) waves, respectively detected in Figure 6.

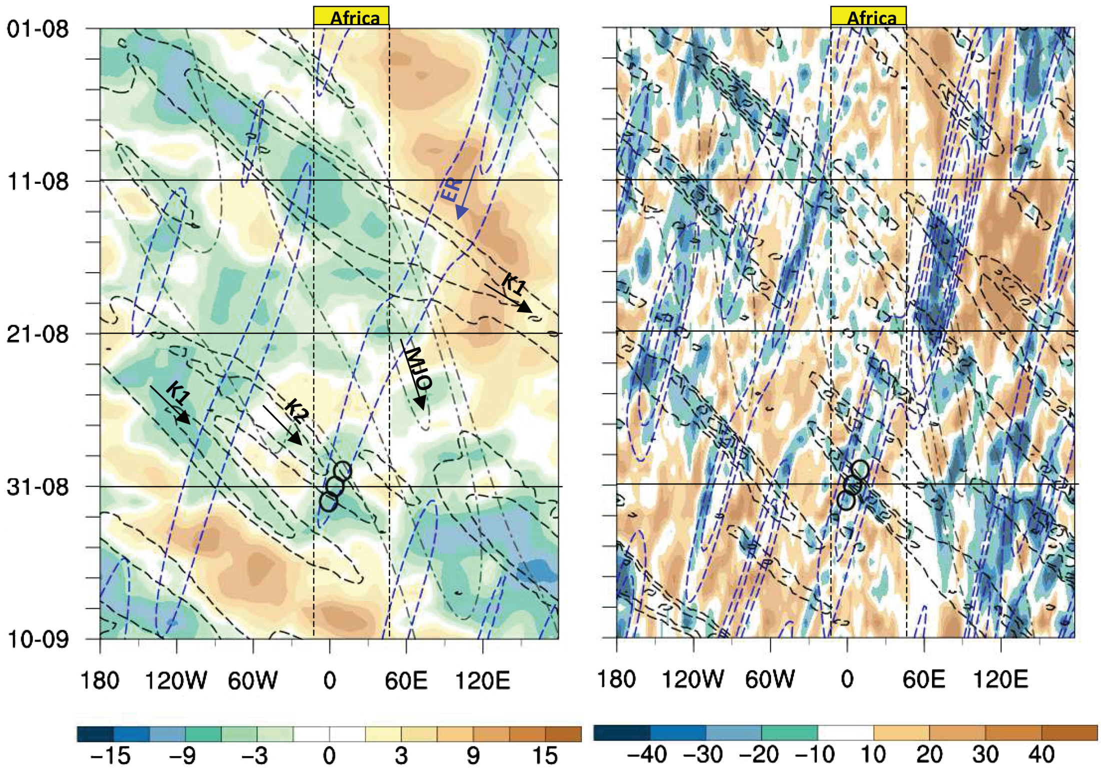

Figure 6. Longitude–time (day-month) diagrams from 1 August to 10 September 2009 of daily anomalies of (a) velocity potential (10^6 m^2 s^{-1}) at 200 hPa and (b) OLR (W m^{-2}). Anomalies are averaged in the 5–15°N band and are relative to the ERA-I and OLR climatologies over the 1979–2014 period. Favourable phases for convection are superimposed for MJO (black dash–dot isolines), Kelvin (black dashes) and Equatorial Rossby waves (blue dashes). Isolines are plotted at −1.5, −3 and -6×10^6 m^2 s^{-1} for (a), and at −5, −10 and −15 W m^{-2} for (b). The three black circles mark the location of the trough T2 on 30, 31 August and 1 September. Africa is delimited by vertical dashed lines (between 15°W and 45°E).

(Figure 4(a)), on the southwestern flank of a widespread wet anomaly (light-grey shading in Figure 4(d)). One day later (Figures 4(b) and (e)) T2 appears as a small-scale cyclonic circulation both at 700 and 925 hPa, such that we have an almost barotropic vortex structure which reaches its maximum on 1 September (Figures 4(c) and (f)). On this date, this vortex located over Niamey has wrapped the wet anomaly which almost splits it into two parts (grey area in Figure 4(f)). A key feature of this event is that contrary to the usual schematic of an AEW (Cornforth *et al.*, 2017 – see their Fig. 2.10) the wet anomaly is ahead (west) of the trough T2 within the northerly flow, instead of being located behind the trough in the monsoon flow. The effect is that the vortex is moistened by the northerly flow. The extreme rain event (coloured shading in Figures 4(c) and (f)) occurred over the Ouagadougou region, 2° west of the vortex within the wet anomaly.

© 2017 Royal Meteorological Society

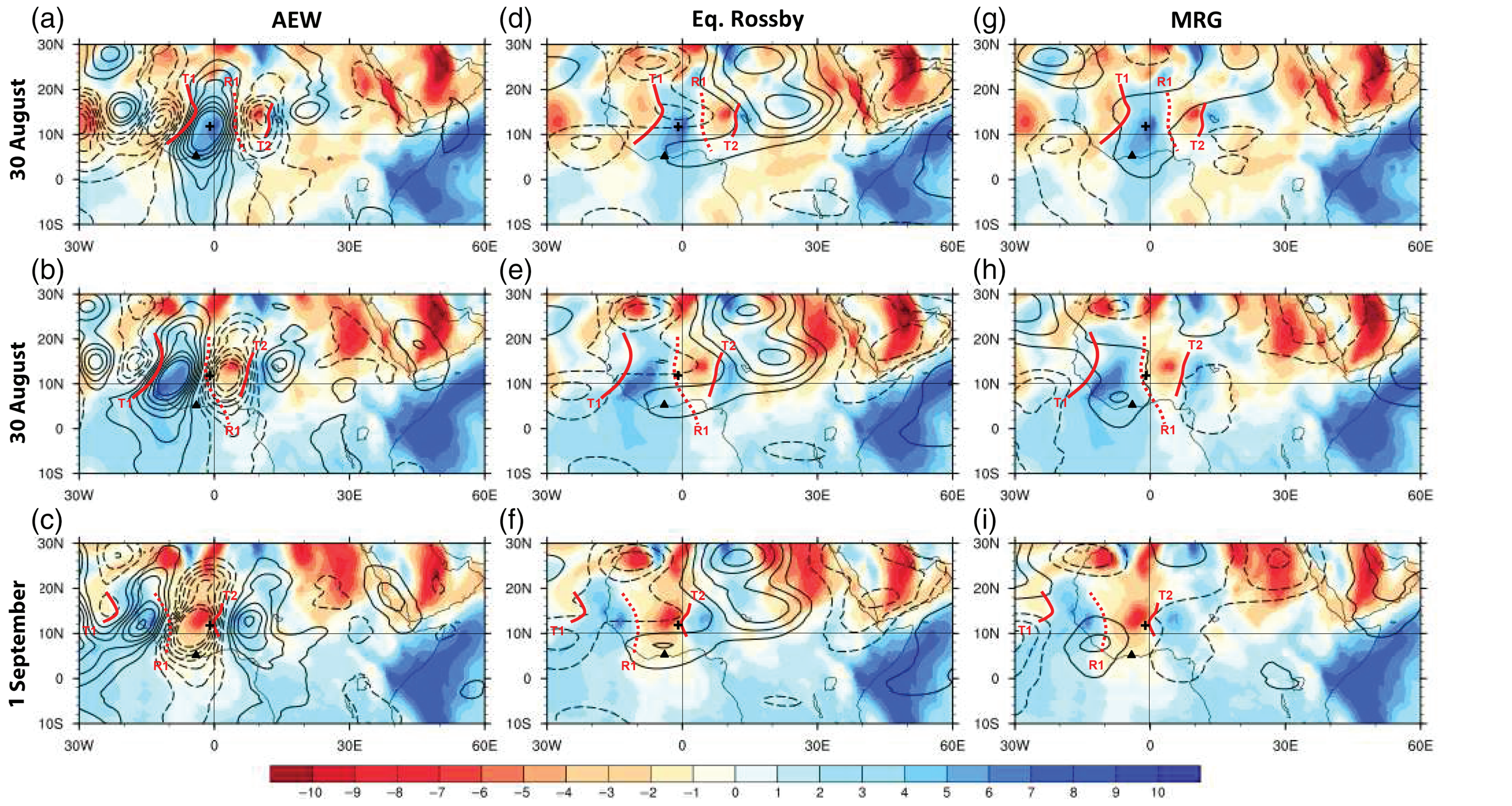

Figure 7. Daily mean maps of the meridional mass transport (colour, in m s^{-1}) defined as the mass-weighted 950–600 hPa layer-averaged meridional wind, with the contributions (isolines, 0.5 m s^{-1} interval, northerlies dashed) of the (a–c) AEW, (d–f) ER and (g–i) MRG waves on (a, d, g) 30 August, (b, e, h) 31 August and (c, f, i) 1 September 2009. The black triangle and cross correspond to the Abidjan and Ouagadougou locations, respectively. The location of troughs T1 and T2 (red solid lines) and ridge R1 (red dashed line) have been superposed on all panels.

To complete, Figure 5 shows a longitude–time diagram zoomed between 40°W and 40°E from 20 August to 10 September for (i) the relative vorticity at 700 hPa, (ii) the anomaly of PW and (iii) the meridional mass transport. Fields are averaged in the Sahelian band 10–18°N. The passage of the train of three AEWs is clearly identified in the vorticity field (Figure 5(a)). The first trough T1 corresponds to the wet spell arrival (Figure 5(b)) and is followed by the strong ridge R1 (anticyclonic vorticity) along the Greenwich meridian. The second trough T2 is even stronger. A day later on 31 August, T2 accelerates and reaches Ouagadougou on 1 September. A third trough T3 intensifies on 4 September near the Greenwich meridian and coincides with the maximum of the wet spell (PW > 60 mm in Figure 5(b)). It is also the most intense trough within the wave train in terms of vorticity signature. This sequence of three successive waves of increasing intensity is consistent with the AEW amplification mechanism due to their upstream group velocity (Diaz and Aiyyer, 2013). T3 later reaches the Atlantic Ocean and gives rise to Hurricane *Fred* on 7 September at 1800 UTC reaching its maximum intensity (958 hPa, 53 m s^{-1}) two days later (see National Hurricane Center report[†]). The trajectory of *Fred* follows the maximum of PW anomalies and vorticity associated with the trough T3 (dotted line T3 in Figure 5). The cyclonic vorticity intensification is in general preceded by a reinforcement of the AEJ (Figure 5(a)), which is consistent with Leroux and Hall (2009), suggesting that an intense AEJ is necessary for intense AEWs to develop. It is to be noticed that the vorticity maximum in the eastern Sahel occurring on 26–27 August corresponds to an AEJ reaching 17.5 m s^{-1}, much stronger than its climatological value from the ERA-I reanalysis (9 m s^{-1}, not shown).

To track the deep southerly burst noted in Figure 4, we computed the meridional mass transport (Figure 5(c)). It provides a clear signature of well-organized AEWs, with the trough located between the deep northerly wind and the southerly deep monsoon flow (to the west and the east, respectively).

4.2. *Equatorial wave activity*

Anomalies of velocity potential at 200 hPa (VP$_{200}$, Figure 6(b)) and of OLR (Figure 6(b)) from 1 August to 10 September 2009 emphasize favourable large-scale conditions for convection prevailing over West Africa, in agreement with Figure 3(a). The analysis of the contributions of equatorial waves (MJO, Kelvin and Rossby) to the anomalies of VP$_{200}$ and of OLR (isolines overlaid in Figure 6) provides additional information. The different signatures obtained using either the VP$_{200}$ or OLR show that the waves are identified slightly differently depending on their life cycle and on the degree of coupling between convection and the dynamics. However, the two panels (Figures 6(a) and (b)) show consistent propagation of the envelope of equatorial waves.

During the first ten days of August, a large divergence anomaly is centred over the eastern Pacific and America, possibly favoured by the intensifying El Niño, whereas a weakly eastward-propagating suppressed convection phase (convergence anomaly) is located over the Indian Ocean. The favourable phase for convection mainly propagates eastward as a convectively coupled Kelvin wave (K1), detected both in VP$_{200}$ and OLR anomaly fields. K1 reaches Africa between 10 and 20 August and is associated with intense convective activity. An MJO signal is also detected over Africa in the middle of August. An equatorial Rossby wave (ER) coming from the Indian Ocean reaches East Africa and then crosses Africa during the last ten days of August. Meanwhile K1 travels from the Maritime Continent to the Atlantic Ocean, where a second Kelvin wave (K2) is generated. The Ouagadougou extreme precipitation event (black circles) coincides with the crossing of the equatorial Rossby wave ER and the Kelvin wave K2. Overall, the MJO signal, which continues eastward over the Maritime Continent, remains weak during the period (after RMM index, not shown). The similar patterns of the waves (Kelvin and ER) detected from the OLR and velocity potential anomalies (Figures 6(b) and (a)) shows that the detection of convectively coupled waves is consistent.

In the present case the AEW wave train corresponds to the passage of the wet spell, and its amplification appears to start after the crossing of the Kelvin wave K2 and the Rossby wave ER (Figures 6 and 5(c)). The following subsection 4.3 analyses the influence of equatorial waves on this extreme event.

4.3. *Connection between equatorial waves and AEWs*

Figure 7 shows maps of meridional mass transport (shading) along with the contribution of ER, MRG and AEW waves to this field (isolines) during the 3-day period from 30 August to 1 September. The evolution of the meridional mass transport shows the propagation of strong northerlies – between R1 and T2 – from 10°E on 30 August to the longitude of Ouagadougou on 1 September, on which the Ouagadougou convective system develops, bordered by strong southerlies to the west and weaker southerlies to the east. As mentioned for Figure 4, the propagation of this dipole of northerly and southerly winds over the Sahel is key to the event and is largely explained by the propagation of an AEW train (Figures 7(a)–(c)). The AEWs even explain a large part of the signal very far into the Southern Hemisphere, down to 10°S, consistent with Kiladis *et al.* (2006), e.g. their Fig. 3. The ER wave which develops further to the east at 15°E (Figures 7(d)–(f)) also contributes to the southerly anomaly, but does not seem to reinforce the AEW at the longitude of the event. This will be further discussed with Figure 8. The MRG wave contributes to the southerlies between T1 and R1 on 30 and 31 August (Figures 7(g) and (h)). It is in phase with the AEW during these two days and thus reinforces the AEW. The maximum contribution of the MRG wave is in the 5–10°N band (Figures 7(g)–(i)), which suggests a possible trapping at the meteorological equator near 7°N (Gill, 1982). Although of weaker magnitude than the AEW, the ER and the MRG waves seem to play a role in building the anomalous southerlies and northerlies, with the MRG and AEW in phase at the longitude of the event, and a possible role of ER further to the east.

The quantitative contribution of each wave to the development of the anomalous southerlies and northerlies is further analysed with Figure 8, which shows zonal profiles of the meridional mass transport and contributions averaged over the 5–15°N band. These allow for a clearer view of the different scales involved in the event.

The ER wave (blue curve in Figure 8) has a zonal wavelength of about 60° and propagates westward at ∼4 m s^{-1}. Its positive phase impacts eastern Africa during the last 10 days of August (in agreement with Figure 6). It drives a mean southerly flow, up to 1.5 m s^{-1}, that may largely contribute to the formation of the wide and long wet spell over the eastern Sahel. For instance, on 27 August (Figure 8(a)) the ER contributes more than the AEW (green curve) to southerlies east of 20°E.

The MRG wave (red curve in Figure 8) has a zonal wavelength of about 40° and propagates westward at ∼6.4 m s^{-1}. Although the MRG wave magnitude is weak (∼1 m s^{-1}) as compared with AEWs (∼4 m s^{-1}), its role in the occurrence of the extreme event of Ouagadougou cannot be neglected. Indeed the two waves (AEW and MRG) propagating at different speeds become in-phase on 30 August (Figure 8(d)), which probably helped the intensification of the ridge R1.

The above wave decomposition (Figures 7 and 8) omits zonal wavelengths shorter than 2000 km, so it cannot explain the whole structure of the present extreme event. For instance on 28 August AEW and ER (green and blue curves in Figure 8(b)) explain only one half of the intense southerly burst (black curve) occurring around 20°E at a scale less than 10°. It is suggested that small-scale processes such as convection may explain this structure associated

[†]http://www.nhc.noaa.gov/data/tcr/AL072009_Fred.pdf.

© 2017 Royal Meteorological Society

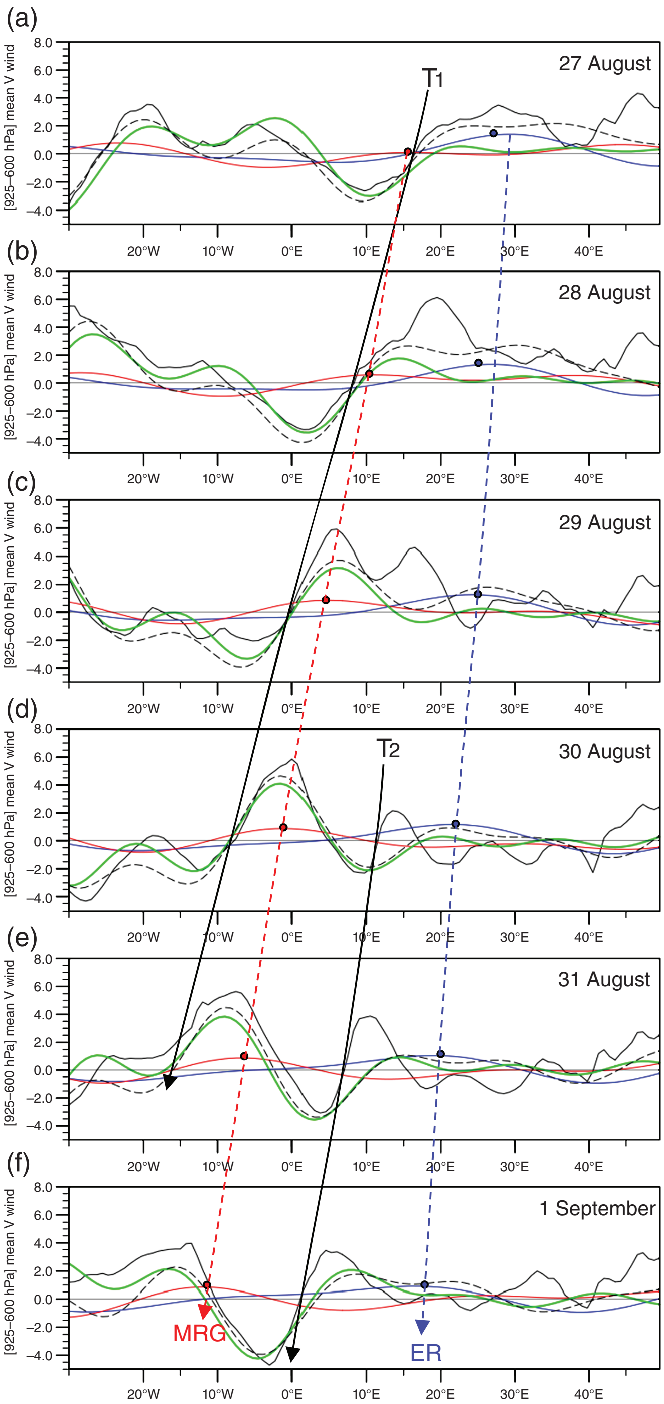

Figure 8. (a–f) Zonal distribution of the meridional mass transport (m s^{-1}) defined as the mass-weighted 950–600 hPa layer-averaged meridional wind, at 0000 UTC averaged in the 5–15°N band (black curve) and the corresponding contributions of the ER (blue), MRG (red) and AEW (green) waves. Black arrows represent the propagation of the AEW troughs T_1 and T_2, whereas blue and red dashed arrows track the maximum of southerly wind associated with ER and MRG waves, respectively. The black dashed line represents the total contribution of ER, MRG and AEW waves. The panel series show the evolution from (a) 27 August to (f) 1 September 2009 at a daily frequency.

with the genesis of the vortex T1 (Hall *et al.*, 2006, their section 5). It is also to be noticed that the arrival of Kelvin wave K2 over the Sahel cannot be seen on the meridional component but it is consistent with the westerly anomaly found ahead of the trough T2 (Figure 4(e)).

The time evolution from 1 August to 10 September of the vertical profile of meridional wind provided by the Abidjan soundings is shown in Figure 9(a). It corresponds to the location where the strong southerly burst reaches its maximum on 30 August. At low levels up to 850 hPa the flow is always northward corresponding to the monsoon and its meridional component reaches 6–7 m s^{-1}. Above, in the 850–500 hPa layer, a large oscillation (with fluctuations between −6 and 10 m s^{-1}) occurs with a maximum amplitude near 700 hPa. Consequently, the southerly burst is mainly due to the deepening of the monsoon layer up to 500 hPa (in particular to the contribution of the 600–750 hPa layer). Figure 9(b) provides a similar time–height series for ERA-I meridional wind averaged in the 0–10°N band. It shows that the reanalysis captures a similar signal over a larger band, which lends confidence to the previous wave-analysis results. Other short-period wave trains are detected above 500 hPa in Figure 9. Further studies will be needed to explain them and their role. A first wave train in the 500–300 hPa layer may contribute to the intensification and deepening of the monsoon flow. The second one at upper levels may be connected to the modulation of the tropical easterly jet (TEJ) through the convective activity of the intertropical convergence zone (ITCZ) (Nicholson *et al.*, 2007).

5. From synoptic to convective scales

5.1. *The breaking signature of the AEW*

The longitude–time diagram of the TRMM rainfall and the ARPEGE 700 hPa meridional wind (Figure 10(a)) illustrates the passage at Ouagadougou of the troughs T1 (30 August, 0000 UTC) and T2 (1 September, 1800 UTC). Between T1 and T2, the ridge R1 is associated with a strong southerly flow whose strength is maximum on 30 August between 1200 and 0000 UTC as already noted in Figure 4. Confirming Figure 4, the latitude–time diagram (Figure 10(b)) shows that the extreme event of Ouagadougou (MCS1) occurred about 12 h before the passage of T2, in the northerly flow (Figure 10(a)), and to the south of the intense AEJ core (Figure 10(b)). The AEW breaking – defined by Cornforth *et al.* (2017) as a very steep north–south oriented curvature of the wave streamlines (Figure 4(c)) – reaches Ouagadougou on 31 August, 1200 UTC (Figure 10(b)). The breaking is so strong that a northwesterly flow at 700 hPa (i.e. overturning) is observed during more than one day south of Ouagadougou (from 31 August 1200 UTC to 2 September at 0000 UTC). After the passage of T2, convection is suppressed during two days before the passage of another MCS (labelled MCS2 in Figure 10(b)) of weaker intensity at the Ouagadougou meridian and linked to AEW3 with an AEJ core located more to the north (16–20°N). This last trough T3 of the AEW train will be the strongest and will be responsible of the genesis of the hurricane *Fred* (Figure 5).

Vertical cross-sections of the relative vorticity field (not shown) and the barotropic structure of the winds (Figures 4 and 9) indicate that the Ouagadougou extreme event corresponds to a deep vortex (AEW2 through T2), which is almost vertically oriented between the surface and 300 hPa, and maximum in the 600–500 hPa layer. To better track this vortex we use the barotropic component of the low-level circulation, being the flow averaged in the 950–600 hPa layer, and analyse the corresponding streamlines, vorticity and wind intensity (Figure 11). This 'barotropic' diagnostic allows an easier detection of strong AEWs. On 29 August, in the lee of AEW1, the initiation of AEW2 over Lake Chad occurs simultaneously with the combination of the AEJ core and the strong southerly flow (Figure 11(a)). During 24 h, AEW2 stays at the same location (2° northwest of Lake Chad) and intensifies. It further evolves into a strong closed circulation isolated from AEW1 (Figures 11(b) and (c)), and propagates westwards (8.2 m s^{-1}) until it reaches the Atlantic on 3 September, 1200 UTC (Figure 11(d)). The vortex size is small, and its intensity of more than 20×10^{-5} s^{-1} (red colour in Figure 11), is maximum during the Ouagadougou event (Figure 11(c)). When reaching Fouta Djalon (10°W, 10°N, Figure 11(d)), the meso-vortex becomes weaker ($\sim 10 \times 10^{-5}$ s^{-1}) but wider.

It is to be noticed that this scenario is reproduced for AEW3 (not shown), which is initiated and intensified in the lee of AEW2 on 3 September at 0000 UTC (see red circle in Figure 11(d) for

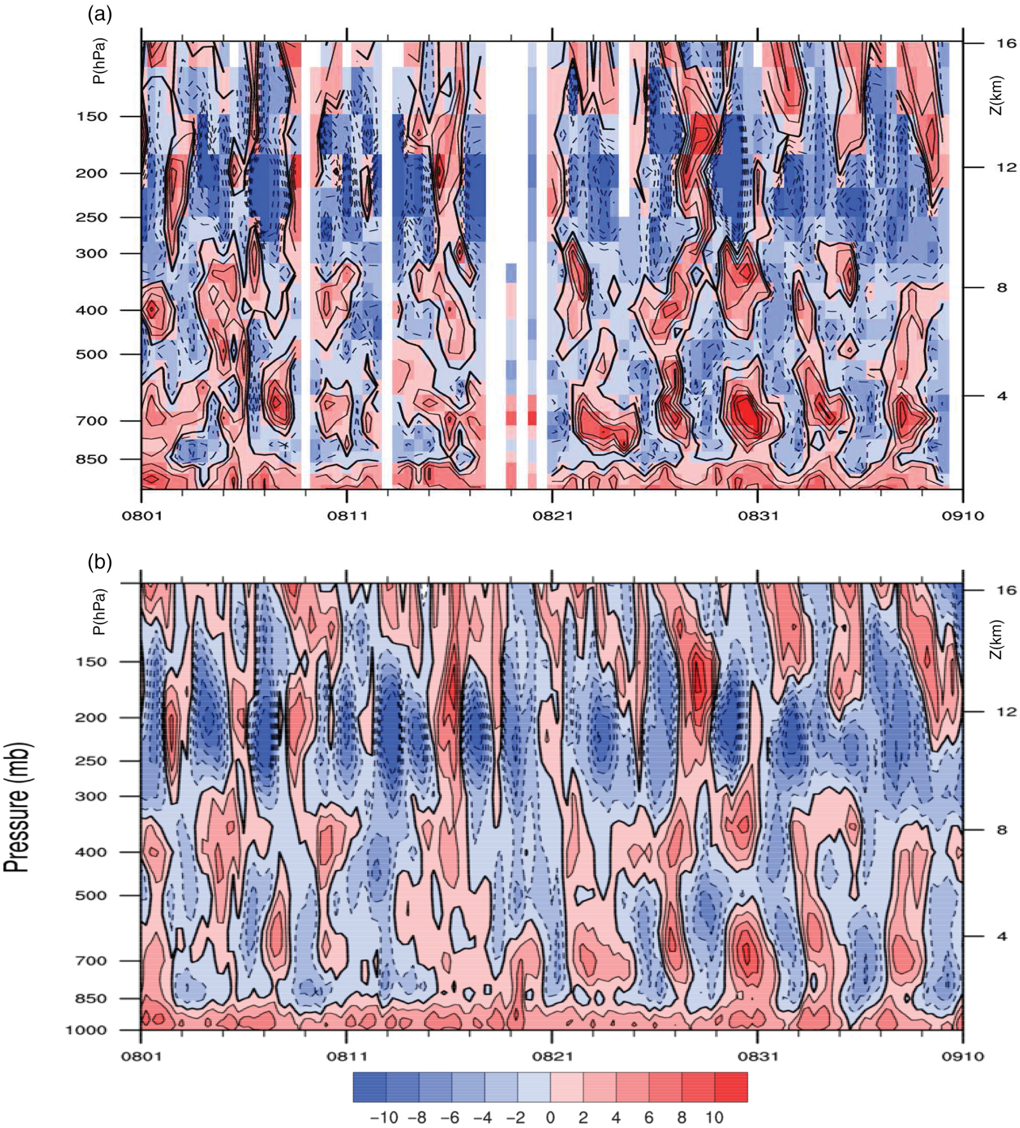

Figure 9. Evolution (month+day) between 1 August and 10 September 2009 of the vertical profile of meridional wind (m s^{-1}) (a) observed twice a day at Abidjan (5.18°N, 4°W), and (b) averaged in the 0–10°N band at the same longitude (4°W) from ERA-I reanalysis.

its location), but at a more northern latitude (16°N, 1°E). During 36 h it intensifies while slowly moving westwards (4.2 m s^{-1}) with the help of a strong ridge as for the previous AEW2 scenario. Then it follows a southwestward trajectory and accelerates (13 m s^{-1}) until it reaches the coast on 6 September at 1200 UTC and where it initiates hurricane *Fred*.

5.2. *Coupling between the vortex and the convection*

To analyse the link between the organized convection and the vortex signature of the Ouagadougou event, Figures 12(a)–(d) show the PCT parameter for a selection of 4 of the 18 AMSR-E, SSMI and TRMM satellite imagery snapshots acquired in the vicinity of the vortex. It corresponds to the sampling of the extreme event of Ouagadougou MCS1 tracked between 31 August at 1733 UTC and 1 September at 1328 UTC. The location of the 'barotropic vortex' AEW2 as detected in Figure 11 is indicated by the black circle. Whereas the infrared (IR) Meteosat images show a large almost circular cloud shield capping MCS1 (not shown), the PCT parameter allows the identification of narrower convective elements (red/black shading) surrounded by widespread stratiform elements (green shading). The second row of Figure 12(e)–(h) provides the corresponding mean wind vector in the 950–600 hPa layer and accumulated rain over 1 h.

On 31 August, the snapshot at 1733 UTC (Figure 12(a)) reveals the structure of a squall line (SL) located ahead of the vortex centre of T2. Figure 12(e) indicates that at 1800 UTC this SL is about 2° west of the vortex, on the southern flank of the AEJ core (solid contour). Six hours later, the narrow arc-shaped band of the SL convective element (black-red shading in Figure 12(b)) is still identified, but now embedded in a widespread area of moderate-to-weak precipitation (yellow to green) as depicted by the snapshot at 0103 UTC. At that time, Ouagadougou (white dot in Figure 12(b)) is at the western edge of the approaching westward-moving SL and the main precipitation area in the southwest sector of the vortex still at a distance of 2° (Figure 12(f)). At 0600 UTC the system appears as a large (4° diameter) 'comma' structure (Figures 12(c) and (g)) with the heaviest convective rains just above Ouagadougou, in the southwest sector of the vortex at a 2° radial distance. To the north the SL is still active ahead of the AEJ core reaching its maximum intensity (Figure 12(c)). At 1200 UTC the convective vortex is slowly decreasing. The snapshot at 1330 UTC (Figure 12(d)) exhibits a large area of moderate precipitation around Ouagadougou, whereas the convective part is over northern Ghana about 3° south of the vortex centre (Figure 12(h)), consistent with the southward track of the MCS1 at the end of its life cycle. This scenario is consistent with the observed rain record described in section 3.1 and in Figure 1(a). The Ouagadougou rainfall peak between 0700 and 0800 UTC (97 mm) corresponds to the slow passage of the intense convective elements seen in Figure 12(c) (red spots).

An analysis of available SYNOP observations at Ouagadougou (not shown, N. Chapelon, 2016; personal communication) showed that the convective system MCS1 was not associated

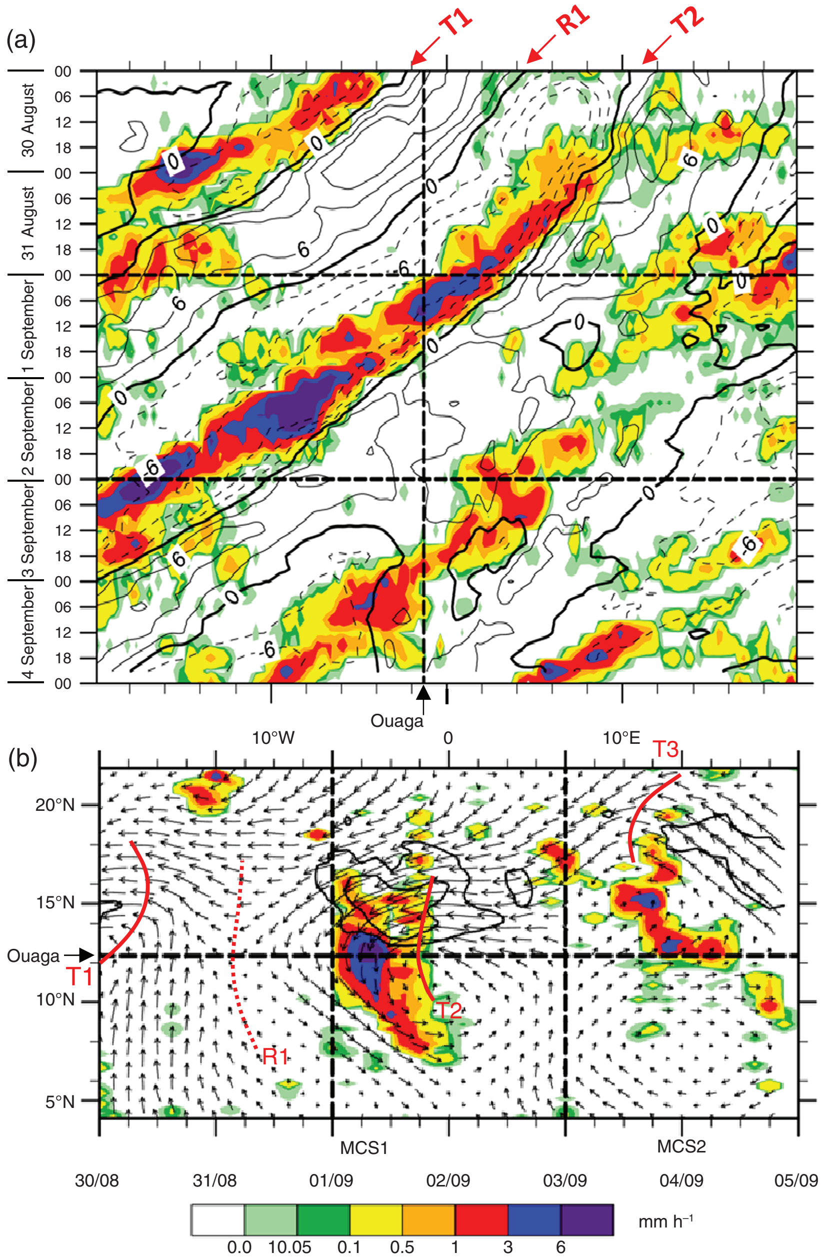

Figure 10. (a) Longitude–time and (b) latitude–time diagrams of 3 h accumulated TRMM rainfall (colour in mm h^{-1}) from 30 August to 4 September 2009. The meridional wind at 700 hPa (isoline in m s^{-1}) of the ARPEGE reanalysis is superposed in panel (a), with northerlies dashed. Horizontal wind vector at 700 hPa is added to panel (b) with isolines of intensity at 15 and 20 m s^{-1} to outline the AEJ core. Fields are averaged in the 10–14°N latitude band for (a) and in the 2.5–0.5°W longitude band for (b) surrounding Ouagadougou. The longitude and latitude of Ouagadougou are indicated by vertical and horizontal dashed lines on panels (a) and (b), respectively. Troughs T1 and T2, and ridge R2 are indicated and labelled in red on both figures.

with surface gusts, nor with convective cold pools, contrary to the typical Sahelian SLs. Indeed the mid-levels were very humid (wet potential temperature $\theta'_w = 23\,°C$) as compared with surface temperature 26 °C, which prevents strong rain evaporation and cold-pool formation as the main driver of the MCS organisation. In contrast with the SL type, the extreme rainfall is associated with a strong meso-vortex, about 2° downshear of its centre, in a region of strong northerly wind. Due to the AEJ, the shear is westward. Such an organisation of convection resembles the conceptual model proposed by Raymond and Jiang (1990) where the diabatic effects of moist convection in a sheared environment can contribute to force vertical motion. A key factor in obtaining this organisation is the pre-existence of a moist anomaly over the northern Sahel. This ensures that northerly wind ahead of the vortex (or of the AEW trough) brings moister air where the ageostrophic forced circulation induces ascent, which supports convection. On the contrary for a Sahelian SL, as northerlies bring drier air, convection is maintained by the cold-pool propagation generated by rain evaporation in the dry air. The companion article will further study the interactions between the mesoscale vortex and the convection using convection-permitting simulations.

6. Summary and conclusion

This first article presents a multi-scale analysis of an extreme rain event that occurred over Burkina Faso on 1 September 2009, with a record for the western Sahel of 263 mm observed at Ouagadougou. Through THORPEX-Africa, daily rain-gauge data from a network of 579 stations over West Africa were collected over a 20-day period centred on 1 September. This dataset is very valuable for the present study and for further ones, in particular to assess the skills of NWP systems to forecast such HIW events.

This case-study occurred during a wet spell phase that crossed the whole Sahel in the last 10 days of August and the first 10 days of September, marked by heavy precipitation leading to floods in many Sahelian countries (e.g. Niger, Senegal, Mauritania, Gambia). Rain-gauge data confirm the intense rainfall activity over West Africa during this period – also associated with the occurrence of a large number of strong events (22) with daily

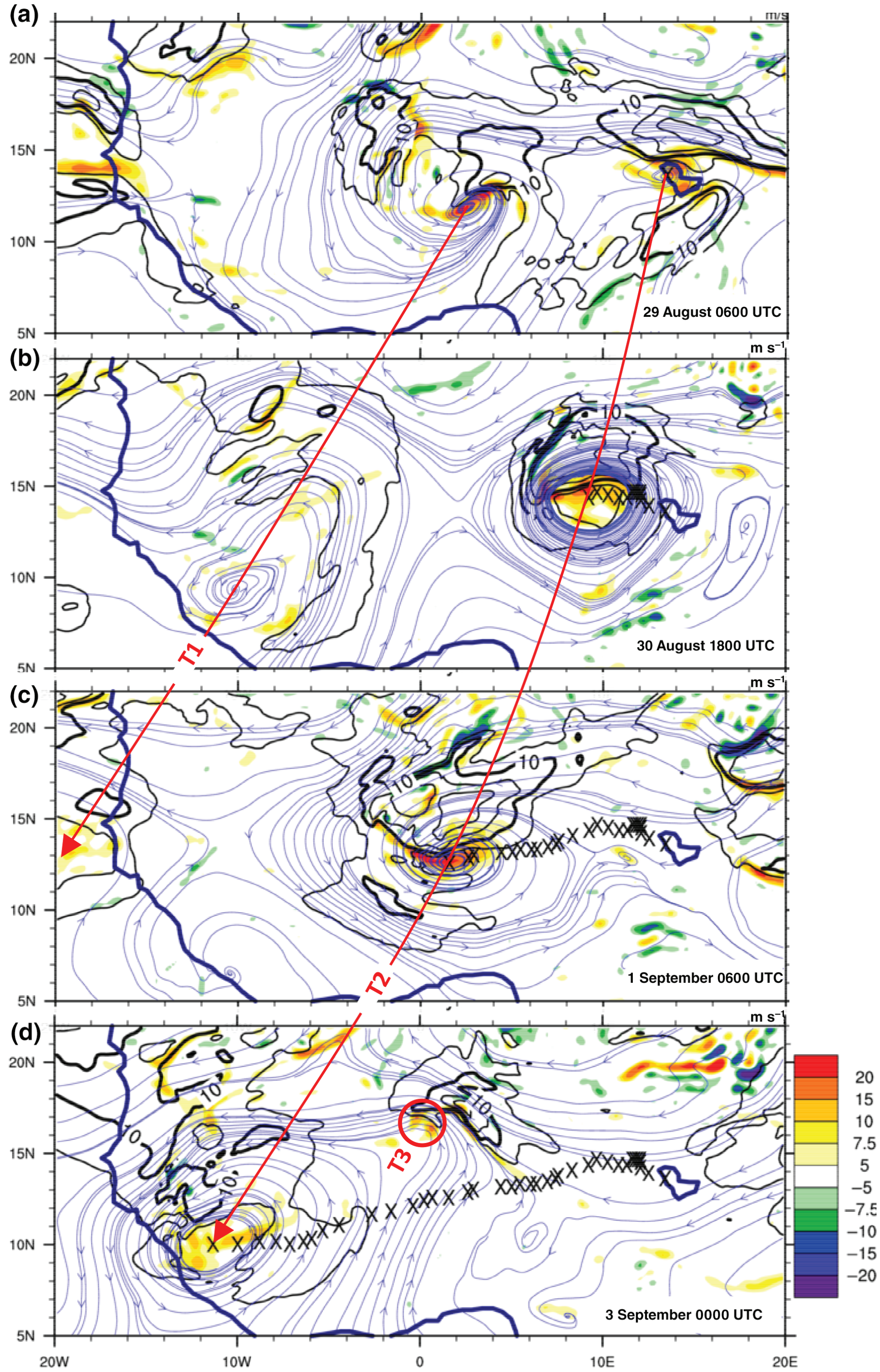

Figure 11. (a–d) Tracking of the vortex associated with AEW2 for the ARPEGE reanalysis as visualized by the streamlines (blue) for the mean flow mass-weighted averaged in the 950–600 hPa layer, with mean horizontal wind speed (black isolines above 7.5 m s^{-1}) and relative vorticity (colour, 10^{-5} s^{-1}). The analysis is performed at 36 h intervals between (a) 29 August at 0600 UTC and (d) 3 September at 0000 UTC. Crosses indicate the location of the vortex centre every 3 h, whereas the red arrows show the progression of the AEW1 and AEW2 troughs. The red circle on panel (d) corresponds to the first detection of T3.

recorded precipitation above 100 mm – producing much more precipitation than the available water vapour typically stored in the atmospheric column (PW_{max} ~65 mm). Although the Ouagadougou precipitation record is the most extreme, it is not isolated. When compared with rain-gauge data, TRMM estimates capture quite well the Ouagadougou extreme event and its trajectory over Burkina Faso. Observed local maxima are, however, underestimated by a factor of two, possibly due to the lower resolution of the TRMM estimate.

The 2009 wet season appears as a wet dipole year over the Sahel as defined by Nicholson (2009). Rainfall is weaker in June and July corresponding to a late onset, but the deficit is made up during the very active period of August–September. It is to be noticed that the footprint of the Ouagadougou extreme event is detected at the seasonal scale, as well as for intense events over Senegal, south Mauritania and Niger.

The SST anomaly patterns in July–August 2009 of the Atlantic cold tongue, the Tropical Atlantic Dipole and the Mediterranean Sea are favourable factors for the WAM northward penetration, and consistent with the classification of 2009 as a dipole wet year. On the contrary, the impact of El Niño, Indian Ocean warming and negative NAO on the WAM are unclear at this point. Nevertheless the Atlantic warm anomaly in the Northern Hemisphere due to the warm phase of the Atlantic Multi-decadal Oscillation appears to favour Sahel precipitation during El Niño as suggested by Rodriguez-Fonseca *et al.* (2011).

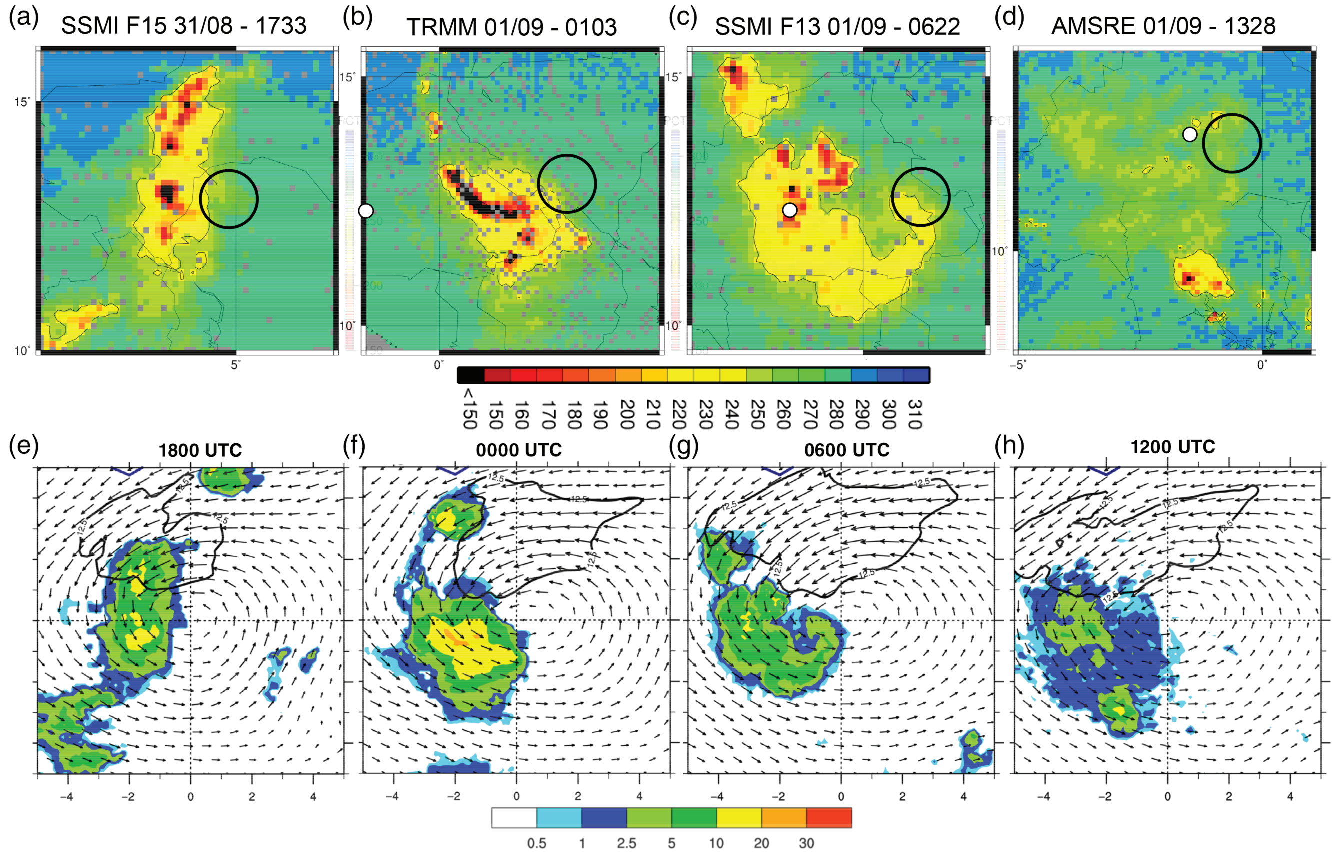

Figure 12. (a–d) Satellite snapshots of the polarized corrected temperature (PCT in °K) in the vortex vicinity indicated by the black circle (times are UTC). Light precipitation (1–3 mm h^{-1}) is delimited by PCT > 255 K (green shading), while convective precipitation (10–12 mm h^{-1}) correspond to PCT < 225 K (warm shading). The white dot corresponds to the Ouagadougou location. The black circle indicates the location of the mean vortex centre as detected by the ARPEGE reanalysis. (e–h) One-day evolution at a 6 h frequency from 31 August 2009 at 1800 UTC of the GSMaP accumulated rain over 1 h (colour in mm) and of the mean wind vector field over the 950–600 hPa layer as analysed by ARPEGE. Maps are drawn relative to the mean vortex centre in a 10° square domain. Heavy black contours outline wind speed higher than 12.5 m s^{-1}.

At synoptic scales the Ouagadougou extreme event was associated with a well pronounced 'breaking' AEW, whose six favourable factors have been identified by forecasters in several case-studies and proposed in the synoptic chapter 2 of the 'West African Forecaster's Handbook' (Cornforth *et al.*, 2017). The present study confirms four of them:

(1) *A pre-existing significant monsoon flow penetration over the eastern Sahel,* resulting in a large-scale wet spell (positive anomaly of PW, Figure 5(b)) over the eastern Sahel, that propagates westward.
(2) *A train of AEWs* (Figures 4 and 5(a)). The trough of the second AEW appears to be reinforced by the first one. A strong ridge develops between them, with drier conditions, which slows down the propagation of the second trough and allows its intensification. This is consistent with the upstream propagation of AEW energy discussed in Diaz and Aiyyer (2013).
(3) *An intense AEJ core* (Figures 4 and 5(a)), associated with the growing second trough.
(4) *Interaction with a deep and intense monsoon flow from the equatorial band.* This monsoon burst can be detected by the southwesterly wind between the surface and 600 hPa, reaching more than 7.5 m s^{-1} (Figure 7).

The last two factors identified by Cornforth *et al.* (2017) (i.e. (5) *Coupling with midlatitudes* and (6) *Intense convective activity to the south of the AEJ*) need further analysis to assess their respective roles for this extreme event.

The present study further suggests additional specific features that may have played a crucial role in favouring the occurrence of this extreme event. At a regional scale the passage of a Kelvin wave (Figure 6) over Africa before the event may have generated favourable conditions for convection (large-scale divergence at 200 hPa, Figure 6(a)), southerly burst (Figure 5(c)) and AEW activity. It is supported by Ventrice *et al.* (2011) who showed that MJO phase 3 is favourable to AEW activity over West Africa and can help in initiating convective systems. The composite study of Ventrice and Thorncroft (2013) concluded that AEW activity increases during and after the passage of the convectively active phase of strong convectively coupled Kelvin waves. This mechanism seems to be at work for the Ouagadougou extreme event (Figure 6). It is also to be noticed that in both studies with a similar Kelvin wave scenario, a hurricane resulted (*Alberto* (2000); *Fred* (2009)).

In the present study, equatorial Rossby waves appear as an important supplementary ingredient whose envelope corresponds to the strong convective activity that crossed Africa westwards during the last 10 days of August. The equatorial Rossby wave passage is associated with a deepening and enhancement of the southerly component of the monsoon flow mainly over the central and eastern Sahel (Figures 7(d)–(f)), which may contribute to generate the large-scale wet spell (factor (1) above). At a finer scale, trapped westward-propagating MRG waves have been detected in the 5–10°N band allowing a modulation of the mean meridional wind in the surface to 600 hPa layer (factor (4) above). Combined with AEW1, MRG waves helped to reinforce the monsoon burst and the associated ridge behind the AEW1 trough on 30 August resulting in the amplification of the AEW2 (factor (2) above).

The precipitating system itself does not resemble a fast-moving squall line which is the dominant type of MCS observed over the Sahel. It corresponds to a moist, slowly-propagating vortex which allows the accumulation of substantial rainfall, while neither surface gust winds nor convective cold pools were observed at the surface. The main precipitation area is located about 2° downshear (westward due to the AEJ) of the centre of this strong meso-vortex, in a region of strong northerly wind. In a companion article we will analyse the physical mechanisms involved in the development of the moist vortex associated with this extreme rain event at a small scale, by using the computation of budgets of heat, moisture and vorticity from a convection-permitting simulation.

This study suggests that this extreme rainfall event results from the combination of several favourable ingredients arising at different scales such as SST patterns, equatorial waves including MJO, Kelvin, ER, MRG and an AEW train, as well as a pre-existing large-scale wet spell. Further studies are necessary to confirm the relative importance of these ingredients and of their combination based on other case-studies of extreme events and on statistical studies. If confirmed, these results may increase our skills in anticipating them, especially if the NWP and climate models are able to represent and forecast those favourable ingredients.

Acknowledgements

This work was supported by the WMO THORPEX programme. The authors would like to acknowledge the NWHSs of the following West African countries: Benin, Burkina Faso, Cape Verde, Ivory Coast, Gambia, Ghana, Guinea-Bissau, Guinea-Conakry, Mauritania, Nigeria, Senegal and Togo for providing precipitation data. We also thank NCAR for the use of the NCL library, in particular for the analysis of equatorial waves. Francoise Guichard and Philippe Peyrillé have received (partial) funding for this research from the UK's National Environment Research Council (NERC)/Department for International Development (DFID) Future Climate For Africa programme, under the AMMA-2050 project (grant number NE/M019950/1). We thank the two anonymous reviewers whose numerous comments and suggestions helped us to improve the text.

References

Arndt DS, Baringer MO, Johnson MR. 2010. State of the climate in 2009. *Bull. Am. Meteorol. Soc.* **91**: S1–S222. https://doi.org/10.1175/BAMS-91-7-StateoftheClimate.

Bader J, Latif M. 2003. The impact of decadal-scale Indian Ocean sea surface temperature anomalies on Sahelian rainfall and the North Atlantic Oscillation. *Geophys. Res. Lett.* **30**: 2169. https://doi.org/10.1029/2003GL018426.

Barthe C, Asencio N, Lafore J-P, Chong M, Campistron B. 2010. Cloud-resolving model simulation of the 25–27 July 2006 convective period over Niamey: Comparison with radar data and other observations. *Q. J. R. Meteorol. Soc.* **136**: 190–208. https://doi.org/10.1002/qj.539.

Benson C, Clay EJ. 1998. 'The impact of drought on sub-Saharan economies', World Bank Technical Paper 401. World Bank: Washington, DC.

Beucher F, Lafore J-P, Karbou F, Roca R. 2014. High-resolution prediction of a major convective period over West Africa. *Q. J. R. Meteorol. Soc.* **140**: 1409–1425. https://doi.org/10.1002/qj.2225.

Birch CE, Parker DJ, O'Leary A, Marsham JH, Taylor CM, Harris PP, Lister GMS. 2013. Impact of soil moisture and convectively generated waves on the initiation of a West African mesoscale convective system. *Q. J. R. Meteorol. Soc.* **139**: 1712–1730. https://doi.org/10.1002/qj.2062.

Caniaux G, Giordani H, Redelsperger JL, Guichard F, Key E, Wade M. 2011. Coupling between the Atlantic cold tongue and the West African monsoon in boreal spring and summer. *J. Geophys. Res.* **116**: C04003. https://doi.org/10.1029/2010JC006570.

Chalon J-P, Gaubert G, Lafore J-P, Roux F. 1988. The West African squall line observed on 23 June 1981 during COPT 81: Mesoscale structure and transports. *J. Atmos. Sci.* **45**: 2744–2763. https://doi.org/10.1175/1520-0469(1988)045<2744:TWASLO>2.0.CO;2.

Chong M. 2010. The 11 August 2006 squall-line system as observed from MIT Doppler radar during the AMMA SOP. *Q. J. R. Meteorol. Soc.* **136**: 209–226. https://doi.org/10.1002/qj.466.

Chong M, Amayenc P, Scialom G, Testud J. 1987. A tropical squall line observed during the COPT81 experiment in West Africa. Part I: Kinematic structure inferred from dual Doppler radar data. *Mon. Weather Rev.* **115**: 670–694.

Cornforth R, Mumba Z, Parker DJ, Berry G, Chapelon N, Diakaria K, Diop-Kane M, Ermert V, Fink AH, Knippertz P, Lafore J-P, Laing A, Lepape S, Maidment R, Methven J, Orji BN, Osika D, Poan E, Roca R, Rowell S, Smith R, Spengler T, Taylor C, Thorncroft C, Vincendon J-C, York C. 2017. Synoptic systems. In *Meteorology of Tropical West Africa: The Forecasters' Handbook*, Parker DJ, Diop-Kane M. (eds.). Wiley: Chichester, UK. https://doi.org/10.1002/9781118391297.ch2.

Courtier P, Thépaut J-N, Hollingsworth A. 1994. A strategy for operational implementation of 4D-Var, using an incremental approach. *Q. J. R. Meteorol. Soc.* **120**: 1367–1387.

Crétat J, Vizy EK, Cook KH. 2015. The relationship between African easterly waves and daily rainfall over West Africa: Observations and regional climate simulations. *Clim. Dyn.* **44**: 385–404. https://doi.org/10.1007/s00382-014-2120-x.

D'Amato N, Lebel T. 1998. On the characteristics of the rainfall events in the Sahel with a view to the analysis of climatic variability. *Int. J. Climatol.* **18**: 955–974.

Dee DP, Uppala SM, Simmons AJ, Berrisford P, Poli P, Kobayashi S, Andrae U, Balmaseda MA, Balsamo G, Bauer P, Bechtold P, Beljaars ACM, van de Berg L, Bidlot J, Bormann N, Delsol C, Dragani R, Fuentes M, Geer AJ, Haimberger L, Healy SB, Hersbach H, Hólm EV, Isaksen L, Kållberg P, Köhler M, Matricardi M, McNally AP, Monge-Sanz BM, Morcrette J-J, Park B-K, Peubey C, de Rosnay P, Tavolato C, Thepaut J-N, Vitart F. 2011. The ERA-Interim reanalysis: Configuration and performance of the data assimilation system. *Q. J. R. Meteorol. Soc.* **137**: 553–597. https://doi.org/10.1002/qj.828.

Descroix L, Genthon P, Amogu O, Rajot J-L, Sighomnou D, Vauclin M. 2012. Change in Sahelian Rivers hydrograph: The case of recent red floods of the Niger River in the Niamey region. *Global Planet. Change* **98–99**: 18–30. https://doi.org/10.1016/j.gloplacha.2012.07.009.

Diaz ML, Aiyyer A. 2013. Energy dispersion in African easterly waves. *J. Atmos. Sci.* **70**: 130–145. https://doi.org/10.1175/JAS-D-12-019.1.

Diongue A, Lafore J-P, Redelsperger J-L, Roca R. 2002. Numerical study of a Sahelian synoptic weather system: Initiation and mature stages of convection and its interactions with the large-scale dynamics. *Q. J. R. Meteorol. Soc.* **128**: 1899–1927.

Enfield DB, Mestas-Nuñez AM. 1999. Multiscale variabilities in global sea surface temperatures and their relationships with tropospheric climate patterns. *J. Clim.* **12**: 2719–2733.

Fink AH, Reiner A. 2003. Spatio-temporal variability of the relation between African easterly waves and West African squall lines in 1998 and 1999. *J. Geophys. Res.* **108**: 4332. https://doi.org/10.1029/2002JD002816.

Giannini A, Saravanan R, Chang P. 2003. Oceanic forcing of Sahel rainfall on interannual to interdecadal time scale. *Science* **302**: 1027–1030.

Gill AE. 1982. *Atmosphere–Ocean Dynamics*. Academic Press: New York, USA.

Grist JP. 2002. Easterly waves over Africa. Part I. The seasonal cycle and contrasts between wet and dry years. *Mon. Weather Rev.* **130**: 197–211.

Grist JP, Nicholson SE, Barcilon AI. 2002. Easterly waves over Africa. Part II. Observed and modelled contrasts between wet and dry years. *Mon. Weather Rev.* **130**: 212–225.

Hall NMJ, Kiladis GN, Thorncroft CD. 2006. Three dimensional structure and dynamics of African easterly waves. Part II: Dynamical modes. *J. Atmos. Sci.* **63**: 2231–2245.

Huffman GJ, Adler RF, Bolvin DT, Gu G, Nelkin EJ, Bowman KP, Hong Y, Stocker EF, Wolff DB. 2007. The TRMM Multisatellite Precipitation Analysis (TMPA): Quasiglobal, multiyear, combined-sensor precipitation estimates at fine scales. *J. Hydrometeorol.* **8**: 3855. https://doi.org/10.1175/JHM560.

Joly M, Voldoire A, Douville H, Terray P, Royer JP. 2007. African monsoon teleconnections with tropical SSTs: Validation and evolution in a set of IPCC4 simulations. *Clim. Dyn.* **29**: 1–20. https://doi.org/10.1007/s00382-006-0215-8.

Karambiri H. 2009. 'Brève analyse fréquentielle de la pluie du 1er septembre 2009 à Ouagadougou (Burkina Faso)', Note technique 2iE, Ouagadougou, Burkina Faso.

Karbou F, Rabier F, Lafore J-P, Redelsperger J-L, Bock O. 2010a. Global 4DVar assimilation and forecast experiments using AMSU observations over land. Part II: Impacts of assimilating surface-sensitive channels on the African monsoon during AMMA. *Weather and Forecasting* **25**: 20–36.

Karbou F, Gerard E, Rabier F. 2010b. Global 4DVar assimilation and forecast experiments using AMSU observations over land. Part I: Impacts of various land surface emissivity parameterizations. *Weather and Forecasting* **25**: 5–19.

Kiladis GN, Thorncroft CD, Hall NMJ. 2006. Three-dimensional structure and dynamics of African easterly waves. Part I: Observations. *J. Atmos. Sci.* **63**: 2212–2230.

Lafore J-P, Chapelon N, Diop-Kane M, Gueye B, Largeron Y, Lepape S, Ndiaye O, Parker DJ, Poan E, Roca R, Roehrig R, Taylor C. 2017. Deep convection. In *Meteorology of Tropical West Africa: The Forecasters' Handbook*, Parker DJ, Diop-Kane M. (eds.): 90–129. Wiley: Chichester, UK. https://doi.org/10.1002/9781118391297.ch3.

Lamb PJ. 1978. Large-scale tropical Atlantic surface circulation patterns associated with Subsaharan weather anomalies. *Tellus* **30**: 240–251.

Le Barbé L, Lebel T, Tapsoba D. 2002. Rainfall variability in West Africa during the years 1950–90. *J. Clim.* **15**: 187–202. https://doi.org/10.1175/1520-0442(2002)015<0187:RVIWAD>2.0.CO;2.

Lebel T, Ali A. 2009. Recent trends in the central and western Sahel rainfall regime (1990–2007). *J. Hydrol.* **375**: 52–64.

Leroux S, Hall NMJ. 2009. On the relationship between African easterly waves and the African easterly jet. *J. Atmos. Sci.* **66**: 2303–2316.

Levinson DH, Lawrimore JH. 2008. State of the climate in 2007. *Bull. Am. Meteorol. Soc.* **89**: 1–179.

Liebmann B, Smith CA. 1996. Description of a complete (interpolated) outgoing longwave radiation dataset. *Bull. Am. Meteorol. Soc.* **77**: 1275–1277.

© 2017 Royal Meteorological Society

Madden R, Julian P. 1971. Detection of a 40–50 day oscillation in the zonal wind in the tropical Pacific. *J. Atmos. Sci.* **28**: 702–708.

Mathon V, Laurent H, Lebel T. 2002. Mesoscale convective system rainfall in the Sahel. *J. Appl. Meteorol.* **41**: 1081–1092.

Mohr K, Zipser EJ. 1996. Defining mesoscale convective systems by their 85 GHz ice-scattering signatures. *Bull. Am. Meteorol. Soc.* **77**: 1179–1189.

Nicholson SE. 2001. Climatic and environmental change in Africa during the last two centuries. *Clim. Res.* **17**: 123–144.

Nicholson SE. 2009. On the factors modulating the intensity of the tropical rainbelt over West Africa. *Int. J. Climatol.* **29**: 673–689. https://doi.org/10.1002/joc.

Nicholson SE, Barcilon AI, Challa M, Baum J. 2007. Wave activity on the tropical easterly jet. *J. Atmos. Sci.* **64**: 2756–2763.

Nka BN, Oudin L, Karambiri H, Paturel JE, Ribstein P. 2015. Trends in floods in West Africa: Analysis based on 11 catchments in the region. *Hydrol. Earth Syst. Sci.* **19**: 4707–4719. https://doi.org/10.5194/hess-19-4707-2015.

Paeth H, Fink AH, Pohle S, Keis F, Mächel H, Samimi C. 2011. Meteorological characteristics and potential causes of the 2007 flood in sub-Saharan Africa. *Int. J. Climatol.* **31**: 1908–1926. https://doi.org/10.1002/joc.2199.

Panthou G, Vischel T, Lebel T, Blanchet J, Quantin G, Ali A. 2012. Extreme rainfall in West Africa: A regional modeling. *Water Resour. Res.* **48**: W08501. https://doi.org/10.1029/2012WR012052.

Panthou G, Vischel T, Lebel T. 2014. Recent trends in the regime of extreme rainfall in the central Sahel. *Int. J. Climatol.* **34**: 3998–4006.

Parker DE, Folland CK, Ward MN. 1988. Sea surface temperature anomaly patterns and prediction of seasonal rainfall in the Sahel region of Africa. In *Recent Climate Change – A Regional Approach*, Chapter 13, Gregory S. (ed.): 166–178. Belhaven Press.

Parker DJ, Diop-Kane M. 2017. *Meteorology of tropical West Africa: The forecasters' handbook*. ISBN: 978-1-118-39130-3, 496, Wiley-Blackwell.

Peyrillé P, Lafore J-P, Redelsperger J-L. 2007. An idealized two-dimensional framework to study the West African monsoon. Part I: Validation and key controlling factors. *J. Atmos. Sci.* **64**: 2765–2782.

Poan E, Roehrig R, Couvreux F, Lafore J-P. 2013. West Africa intraseasonal variability: A precipitable water perspective. *J. Atmos. Sci.* **70**: 1035–1052. https://doi.org/10.1175/JAS-D-12-087.1.

Raymond DJ, Jiang H. 1990. A theory for long-lived mesoscale convective systems. *J. Atmos. Sci.* **47**: 3067–3077. https://doi.org/10.1175/1520-0469(1990)047<3067:ATFLLM>2.0.CO;2.

Redelsperger J-L, Lafore J-P. 1988. A three-dimensional simulation of a tropical squall line: Convective organization and thermodynamic vertical transport. *J. Atmos. Sci.* **45**: 1134–1356.

Redelsperger J-L, Diongue A, Diedhiou A, Ceron J-P, Diop M, Gueremy J-F, Lafore J-P. 2002. Multi-scale description of a Sahelian synoptic weather system representative of the West African monsoon. *Q. J. R. Meteorol. Soc.* **128**: 1229–1257. https://doi.org/10.1256/003590002320373274.

Reynolds RW, Rayner NA, Smith TM, Stokes DC, Wang W. 2002. An improved in situ and satellite SST analysis for climate. *J. Clim.* **15**: 1609–1625.

Rodriguez-Fonseca B, Janicot S, Mohino E, Losada T, Bader J, Caminade C, Chauvin F, Fontaine B, García-Serrano J, Gervois S, Joly M, Polo I, Ruti P, Roucou P, Voldoire A. 2011. Interannual and decadal SST-forced responses of the West African monsoon. *Atmos. Sci. Lett.* **12**: 67–74. https://doi.org/10.1002/asl.308.

Roundy PE, Frank WM. 2004. A climatology of waves in the equatorial region. *J. Atmos. Sci.* **61**: 2105–2132.

Roux F. 1988. The West African squall line observed on 23 June 1981 during COPT81: Kinemaric and thermodynamics of the convective region. *J. Atmos. Sci.* **45**: 406–426.

Rowell DP. 2003. The impact of Mediterranean SSTs on the Sahelian rainfall season. *J. Clim.* **16**: 849–862.

Schreck C, Molinari J, Aiyyer A. 2012. A global view of equatorial waves and tropical cyclogenesis. *Mon. Weather Rev.* **140**: 774–788. https://doi.org/10.1175/MWR-D-11-00110.1.

Schwendike J, Jones SC. 2010. Convection in an African easterly wave over West Africa and the eastern Atlantic: A model case study of Helene (2006). *Q. J. R. Meteorol. Soc.* **136**: 364–396.

Servain J. 1991. Simple climatic indices for the tropical Atlantic Ocean and some applications. *J. Geophys. Res.* **96**: 137–146. https://doi.org/10.1029/91JC01046.

Sighomnou D, Descroix L, Genthon P, Mahé G, Moussa IB, Gautier E, Mamadou I, Vandervaere JP, Bachir T, Coulibaly B, Rajot JL, Malam-Issa O, Malam-Abdou M, Dessay N, Delaitre E, Faran-Maiga O, Diedhiou A, Panthou G, Vischel T, Yacouba H, Karambiri H, Paturel JE, Diello P, Mougin E, Kergoat L, Hiernaux P. 2013. La crue de 2012 á Niamey: Un paroxysme du paradoxe du Sahel? *Sécheresse* **24**: 3–13.

Takayabu YN. 1994. Large-scale cloud disturbances associated with equatorial waves. Part I: Spectral features of the cloud disturbances. *J. Meteorol. Soc. Jpn.* **72**: 433–448.

Taylor CM, Belušić D, Guichard F, Parker DJ, Vischel T, Bock O, Harris PP, Janicot S, Klein C, Panthou G. 2017. Frequency of extreme Sahelian storms tripled since 1982 in satellite observations. *Nature* **544**: 475–478. https://doi.org/10.1038/nature22069.

Thiaw WM. 2013. (West Africa) sidebar 7.3 Africa: The floods of the Sahel in 2012 In 'State of the climate in 2012'. *Bull. Am. Meteorol. Soc.* **94**: S164–S165.

Ushio T, Sasashige K, Kubota T, Shige S, Okamoto K, Aonashi K, Inoue T, Takahashi N, Iguchi T, Kachi M, Oki R, Morimoto T, Kawasaki Z. 2009. A Kalman filter approach to the Global Satellite Mapping of Precipitation (GSMaP) from combined passive microwave and infrared radiometric data. *J. Meteorol. Soc. Jpn.* **87A**: 137–151.

Ventrice MJ, Thorncroft CD. 2013. The role of convectively coupled atmospheric Kelvin waves on African easterly wave activity. *Mon. Weather Rev.* **141**: 1910–1924. https://doi.org/10.1175/MWR-D-12-00147.1.

Ventrice MJ, Thorncroft CD, Roundy PE. 2011. The Madden–Julian Oscillation's influence on African easterly waves and downstream tropical cyclogenesis. *Mon. Weather Rev.* **139**: 2704–2722. https://doi.org/https://doi.org/10.1175/MWR-D-10-05028.1.

Westra S, Fowler HJ, Evans JP, Alexander LV, Berg P, Johnson F, Kendon EJ, Lenderink G, Roberts NM. 2014. Future changes to the intensity and frequency of short-duration extreme rainfall. *Rev. Geophys.* **52**: 522–555. https://doi.org/10.1002/2014RG000464.

Wheeler MC, Hendon HH. 2004. An all-season real-time multivariate MJO index: Development of an index for monitoring and prediction. *Mon. Weather Rev.* **132**: 1917–1932. https://doi.org/10.1175/1520-0493(2004)132<1917:AARMMI>2.0.CO;2.

Wheeler MC, Kiladis GN. 1999. Convectively coupled equatorial waves: Analysis of clouds and temperature in the wavenumber–frequency domain. *J. Atmos. Sci.* **56**: 374–399.

© 2017 Royal Meteorological Society